2

Synthesis of Diamond Using Spark Plasma Sintering

Faming Zhang and Eberhard Burkel
Physics of New Materials,
University of Rostock, Rostock
Germany

1. Introduction

Carbon is a complex system rich in polymorphs due to its ability to form sp^1-, sp^2-, and sp^3-hybridized C-C bonds. One of the most outstanding achievements in carbon science was the synthesis of diamond from graphite under high-pressure and high-temperature (HPHT) conditions (Giardini et al., 1960). Since diamond particles and films have now been obtained by many other methods including detonation (Vereschagin et al., 1994), combustion flames (Hirose et al., 1990) and chemical vapour deposition (CVD) with RF plasma (Watanabe et al., 1992) or microwave plasma (Kobashi et al., 1988) etc., the HPHT method is still the most popular commercial method for the diamond synthesis. Nowadays, man-made diamond plays an indispensable role in modern industry for abrasives, tool coatings, microelectronics, optics and other applications.

Spark plasma sintering (SPS), commonly also defined as field assisted sintering (FAST) or pulsed electric current sintering (PECS) is a novel pressure assisted pulsed electric current sintering process utilizing ON-OFF DC pulse energizing. Due to the repeated application of an ON-OFF DC pulse voltage and current in powder materials, the spark discharge point and the Joule heating point (local high temperature-state) are transferred and dispersed to the overall specimen (Zhang & Burkel, 2010). The SPS process is based on the electrical spark discharge phenomenon: a high energetic, low voltage spark pulse current momentarily generates high localized temperatures, from several to ten thousand degrees between the particles resulting in high thermal and electrolytic diffusion. During SPS treatment, powders contained in a die can be processed for diverse novel bulk material applications, for example nanostructured materials, functional gradated materials, hard alloys, biomaterials, porous ceramics and alloys etc (Zhang & Burkel, 2010). The SPS has been used to prepare diverse advanced materials; nevertheless, it is still a new technique for the diamond synthesis.

In the year 2004, during the study of the thermal stability of multi-walled carbon nanotubes (MWCNTs) under various SPS conditions, Zhang et al first found that under SPS conditions of 1500 ^{o}C at very low pressure (80 MPa) carbon nanotubes were unstable and transformed into diamonds without any catalysts being involved (Zhang, Shen et al., 2005). The transformation mechanism involves the breakage of some C–C bonds, the formation of carbon nano-onions (multilayer fullerenes), and the nucleation and growth of the diamond

phase within the onion cores (Shen, Zhang et al., 2006). The effect of the high temperatures and sparking plasmas is akin to the electron or ion beam irradiations or high pressures. As a result, diamond forms from the intermediate nano-onions when localized high energy conditions are satisfied (Shen, Zhang et al., 2006). Additionally, the low purity MWCNTs (60% purity) with a very cheap price also can be used as starting materials for the direct synthesis of diamond by the SPS technique (Zhang, Shen et al., 2006). It is postulated that the spark plasmas play a key role to provide most of the energy required in these diamond transitions. It is seen as an important evidence for the presence of spark plasmas during the SPS process. These studies indicate that the SPS has a potential to be used as an alternative method for diamond generation. But it needs further investigation to promote the SPS method to be used as a large-scale synthetic diamond production technique instead of the present hydrostatic HPHT method.

This chapter will focus on the synthesis of diamond using the SPS technique. We aim to promote the SPS method to be used as a large-scale synthetic diamond production technique as an alternative to the present HPHT method. In the first part of this chapter, the thermal stability of carbon nanotubes, C60 and graphite under the pulsed DC field of SPS and AC field of conventional sintering will be studied. In the second part of this chapter, the application of catalysts in the diamond synthesis by the SPS will be investigated. In the last part of this chapter, the factors that influence the diamond growth in the SPS, including carbon modifications and atmospheres (Vacuum, Ar) will be studied in order to increase the diamond sizes and transition rates.

2. Major raw materials and methods

- The MWCNTs with purity above 95.0% were obtained from Shenzhen Nanotech Port, Ltd., China. The C60 powders with purity of 99.5% were obtained from SES Research, Huston, USA. The graphite powders with purity of 99.0% were purchased from Alfa Aesar, Germany.
- The catalyst powders of Fe-35Ni, Ni etc. were purchased from Alfa Aesar, Germany. They were prepared by gas atomization method with 99.0% purity.
- The SPS experiments were conducted using a Model HP D-125/5 FCT spark plasma sintering system (FCT systeme GmbH, Rauenstein, Germany) installed in our Tycho Sinter Lab at the University of Rostock, Germany. The powders were pressed into a ф20 mm graphite die for the SPS treatment to form disk-shaped samples with thickness of 5-8 mm.
- The sintered samples were etched in a boiling solution of concentrated H_2SO_4 (90 vol.%) and HNO_3 (10 vol.%) for 2 h. The etched samples were washed using deionized water repeatedly, and dried in a vacuum oven.
- The phase identification of the etched carbon samples was performed using high-energy X-ray diffraction with energies of 80-100 keV at beamline BW5 (DESY/HASYLAB Hamburger Synchrotron Laboratory). The carbon samples were also analyzed by a Renishaw-2000 Laser Raman spectroscopy system with a He–Ne laser excited at 512 nm to identify the diamond phase.
- Scanning electron microscope (SEM, Zeiss Supra 25, Germany) and transmission electron microscope (TEM, Zeiss-Libra120, Germany) operating at 120 keV, were employed to characterize the products following the SPS treatment.

- The comparison investigation on the stability of the carbon materials was conducted by the in-situ high temperature X-ray diffraction at the MAX80/F2.1 high-pressure beamline of Helmholtz Centre Potsdam at HASYLAB/DESY Hamburg.

3. Stability of carbon nanotubes, C60 and graphite under various fields

The transformation of carbon nanotubes to diamond at very low pressure under SPS has been observed for the first time by Zhang, Shen et al. (2004). Recently, Inam et al reported that multiwall carbon nanotubes were not preserved for ceramic matrices that require high sintering temperatures (>1600°C) and longer processing times (>13 min) in the SPS (Inam et al., 2010). Zhang et al proposed that the spark plasmas may play a key role to provide most of the energy required in this diamond transition, and it provided an indirect way to validate the existence of the plasmas during the SPS. Due to the still on-going arguments about whether the spark plasmas actually occur during the SPS process (Anselmi-Tamburini et al., 2005, Hulbert et al., 2008), it needs further investigations on this point. In this part, we used such an indirect way to prove the presence of plasmas during the SPS. The thermal stability and phase transitional behaviour of carbon nanotubes, C60 and graphite were investigated under the SPS (pulsed DC field). For a comparison study, these carbon materials were also studied using the in-situ high temperature (AC field) synchrotron radiation X-ray diffraction.

3.1 Stability and phase transformation of carbon materials under pulsed DC field

The pure MWCNTs were SPSed at 1500 ^{o}C under pressure of 80 MPa for a holding time of 20 min. Figure 1(a) shows the synchrotron radiation-high energy X-ray diffraction patterns of the raw MWCNTs and the spark plasma sintered (SPSed) MWCNTs. The raw MWNCTs show a main diffraction peak at 3.43 Å corresponding to the CNTs (002) plane spacing, and weak peaks at 2.10 and 1.70 Å corresponding to the CNTs (100) and (004) plane spacing, respectively. After SPS processing, the MWCNTs diffraction peaks are still present in the sintered MWCNTs compacts, but the peaks of the CNTs (002), (100) and (004) are stronger than those in the raw MWCNTs. It indicates that the SPS process improved the crystallinity of the MWCNTs (Zhang, Mihoc et al., 2011). Additionally, new peaks were detected in the sample centered at 2.05, 1.23, 1.06 and 1.76 Å corresponding to the cubic diamond (ICDD No. 65-537) (111), (220), (311) and n-diamond (ICDD No. 43-1104) (200) plane spacing, respectively. Figure 1(b) shows the Raman spectra of the raw MWCNTs and the SPSed MWCNTs. The result of the raw MWCNTs show that their D band appeared at 1344 cm^{-1} and G band appeared at 1569 cm^{-1}. After SPS processing, the D peak shifted to 1333 cm^{-1} corresponding to the cubic diamond but there was still a weak peak at 1344 cm^{-1} belonging to the un-reacted MWCNTs, the G band shifted to 1566 cm^{-1} relating to the sp^2 bonded carbon vibrations. The results of the X-ray diffraction and Raman spectroscopy confirmed the diamond formation in the MWCNTs sample after SPS at 1500 ^{o}C under 80 MPa for 20 min.

Figure 2 shows the SEM micrographs of the raw MWCNTs and the spark plasma sintered MWCNTs at 1500 ^{o}C under 80 MPa for 20 min. The fibrous structures of the raw MWCNTs can be observed in the Figure 2(a). But these structures have disappeared, and some diamond crystals are found in the samples after SPS. Figure 2 (b) shows one diamond crystal with particle size of 35 μm around. In the background of this diamond crystal, no MWCNTs are found.

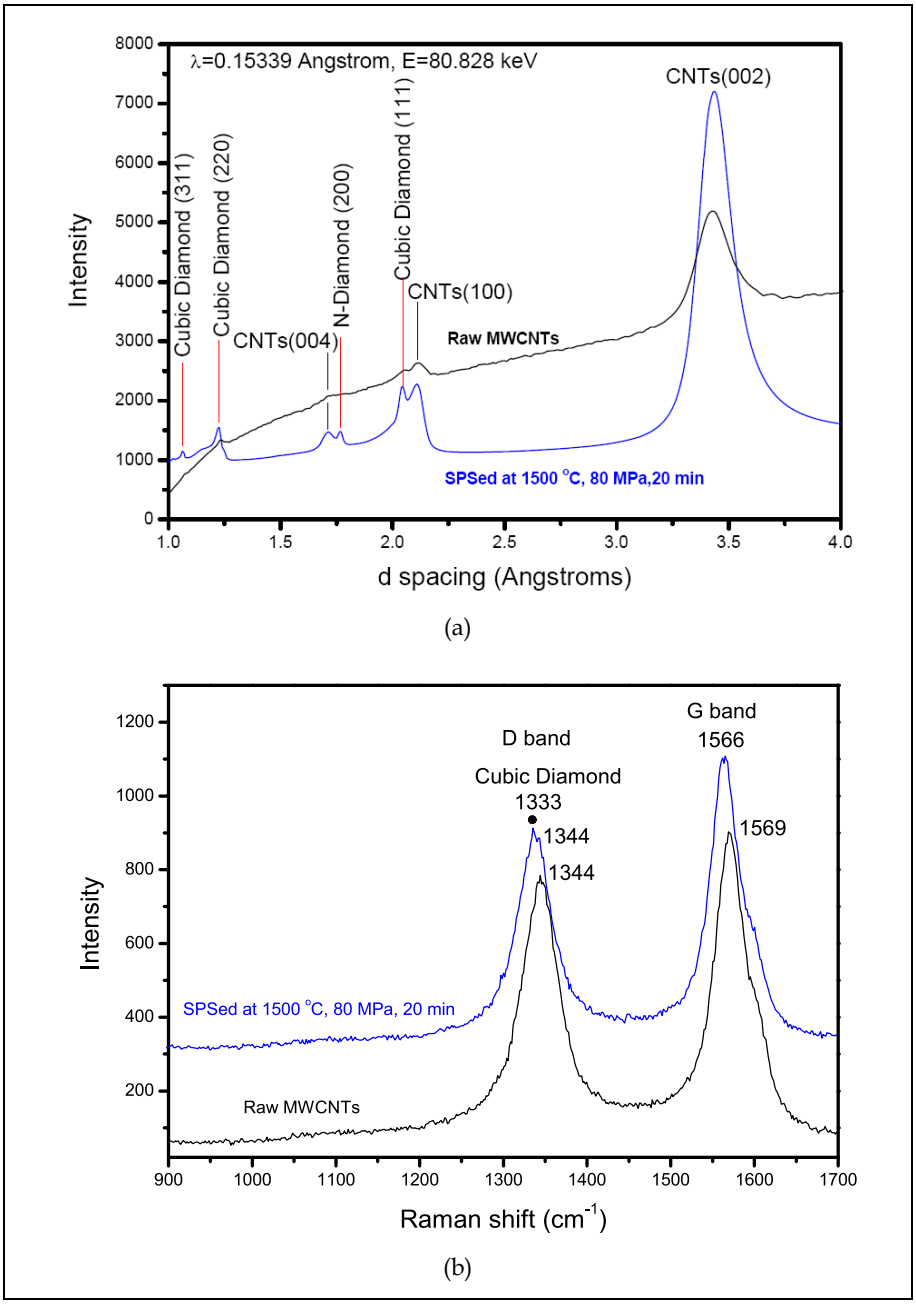

Fig. 1. Synchrotron radiation-high energy X-ray diffraction patterns (a) and Raman spectra (b) of the raw MWCNTs and the spark plasma sintered MWCNTs at 1500 ◦C, 80 MPa for 20 min.

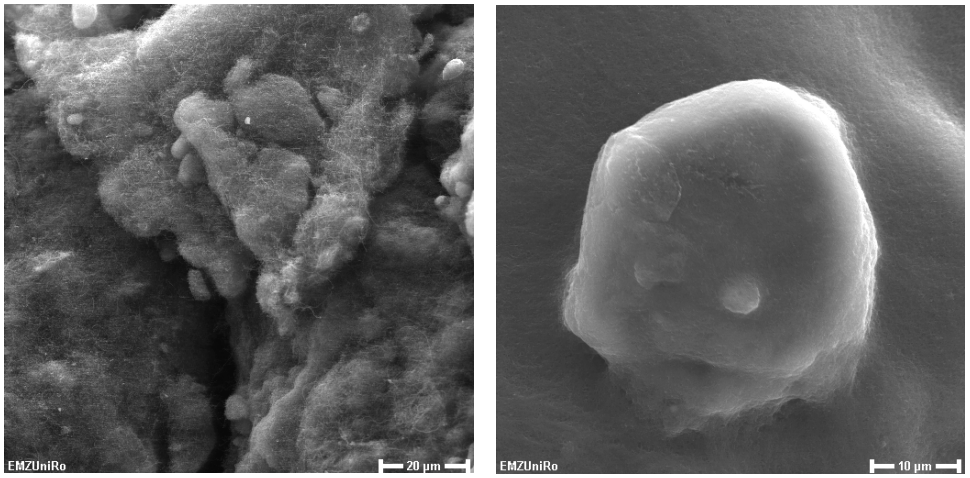

(a) (b)

Fig. 2. SEM micrographs of the raw MWCNTs (a) and the spark plasma sintered MWCNTs at 1500 °C, 80 MPa for 20 min showing one diamond crystal (b).

Figure 3(a) shows the synchrotron radiation-high energy X-ray diffraction patterns of raw C60 and the SPSed C60 at 1500 °C, 80 MPa for 20 min. The raw C60 exhibits diffraction peaks at d spacing of 5.01, 4.28, 4.11, 3.18, 2.9, 2.74 Å belonging to C60 (110), (112), (004), (114), (300), (006) planes (ICDD No. 47-0787), respectively. The C60 after SPS shows the cubic diamond diffraction peaks at d spacing of 2.06 and 1.23 Å and a broad graphite peak. The C60 diffraction peaks disappeared indicating the C60 has completely transformed into diamond and graphite phases after the SPS processing. Figure 3(b) shows the Raman spectra of the raw C60 and the SPSed C60. The raw C60 shows a sharp peak appearing at 1460 cm^{-1}, and two weak, broad peaks centered at 1568 and 1515 cm^{-1}. After SPS processing, it shows the cubic diamond peak at 1333 cm^{-1} and graphite peak at 1558 cm^{-1}, but the C60 peak at 1460 cm^{-1} disappeared. It is consistent with X-ray diffraction results that the C60 has completely transformed into diamond and graphite phases after SPS at 1500 °C under 80 MPa for 20 min.

Figure 4 shows the SEM micrographs of the raw C60 and the spark plasma sintered C60 at 1500 °C under 80 MPa for 20 min. The raw C60 powders are nano-particle agglomerates and show bundles of C60 in the Figure 4(a). Some diamond crystals with sizes from 2 to 8 µm can be observed in the Figure 4(b). The structures of C60 are not noticeable in the background of the diamond crystals.

Figure 5 (a) shows the synchrotron radiation diffraction patterns of the raw graphite and the SPSed graphite at 1500 °C under 80 MPa for 20 min. The raw graphite sample presents Graphite-3R and Graphite-2H diffraction peaks those are centered at 3.348 Å [G-3R(003)], 1.674 Å [G-3R(006)], 1.228 Å [G-3R(110)] (ICDD No. 26-1079), and 2.138 Å [G-2H(100)] , 2.039 Å [G-2H(101)], 1.16 Å [G-2H(112)] (ICDD No. 41-1487). However, the diamond phase is not found in the graphite samples after the SPS processing. Only, an increased intensity in the

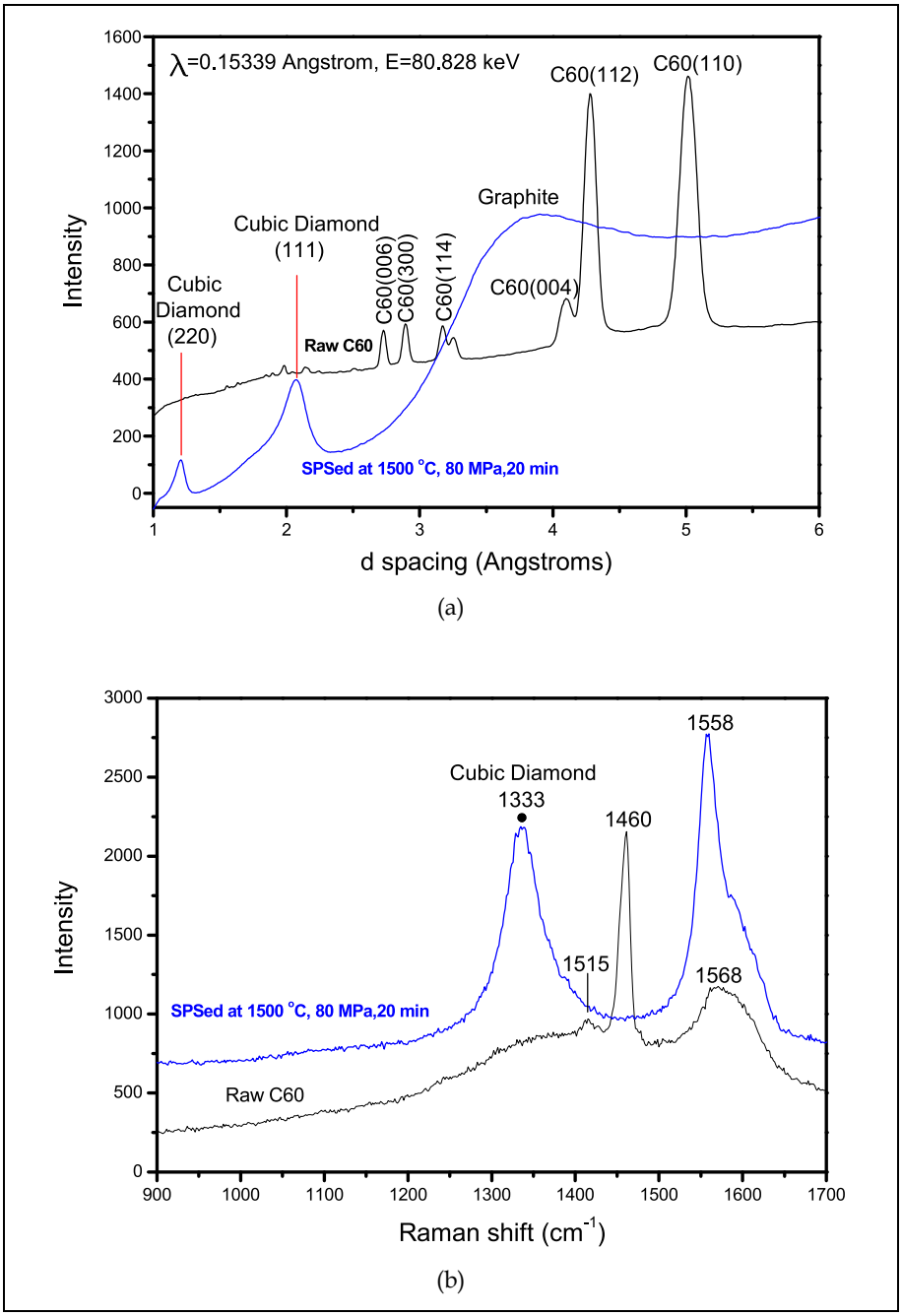

Fig. 3. Synchrotron radiation-high energy X-ray diffraction patterns (a) and Raman spectra (b) of the raw C60 and the spark plasma sintered C60 at 1500 °C, 80 MPa for 20 min.

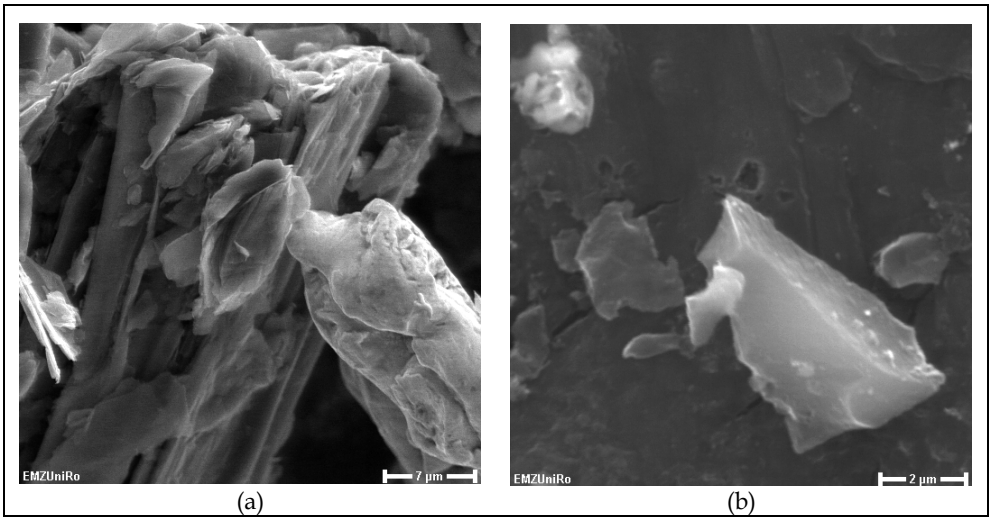

Fig. 4. SEM micrographs of the raw C60 (a) and the spark plasma sintered C60 at 1500 °C, 80 MPa for 20 min (b).

graphite peaks indicating the improved crystallinity is visible. Figure 5(b) shows the Raman spectra of the raw graphite and the SPSed graphite. The raw graphite shows a sharp peak at 1579 cm^{-1}, and a weak peak at 1350 cm^{-1}. After SPS processing, the intensity of the peak at 1350 cm^{-1} has improved, but there is no diamond peak in the Raman spectra. The X-ray diffraction and Raman spectroscopy results confirmed that there is no diamond conversion from pure graphite after SPS at 1500 °C under 80 MPa for 20 min.

Fig. 6 shows the SEM micrographs of the raw graphite and the spark plasma sintered graphite at 1500 °C under 80 MPa for 20 min. The raw graphite shows the typical layered structure as shown in Figure 6(a). After the SPS of MWCNTs and C60 at the identical condition, there is no presence of diamond in the sample (Figure 6b). The sample shows the similar structure as the raw graphite. The SEM results agree well with the XRD and Raman results and confirmed that there is no diamond conversation from pure graphite after SPS at 1500 °C under 80 MPa for 20 min.

3.2 Stability and phase transformation of carbon materials under AC field

Figure 7 (a) shows the synchrotron radiation-in situ X-ray diffraction patterns of the pure MWCNTs at 80 MPa under different temperatures. In the in-situ sintering furnace (AC filed) of the MAX80/F2.1 high-pressure beamline. The combining peak of MWCNT and graphite has shifted to lower energy values. It indicates the thermal expansion of the nanotubes and graphite planes with the increase of temperature. The boron nitride (BN) peaks are from the container of the powder sample during the in-situ high temperature X-ray experiments. However, there is no diamond formation at or below the temperature of 1500 °C under 80 MPa. This means that the MWCNTs are dynamically stable at this temperature 1500 °C

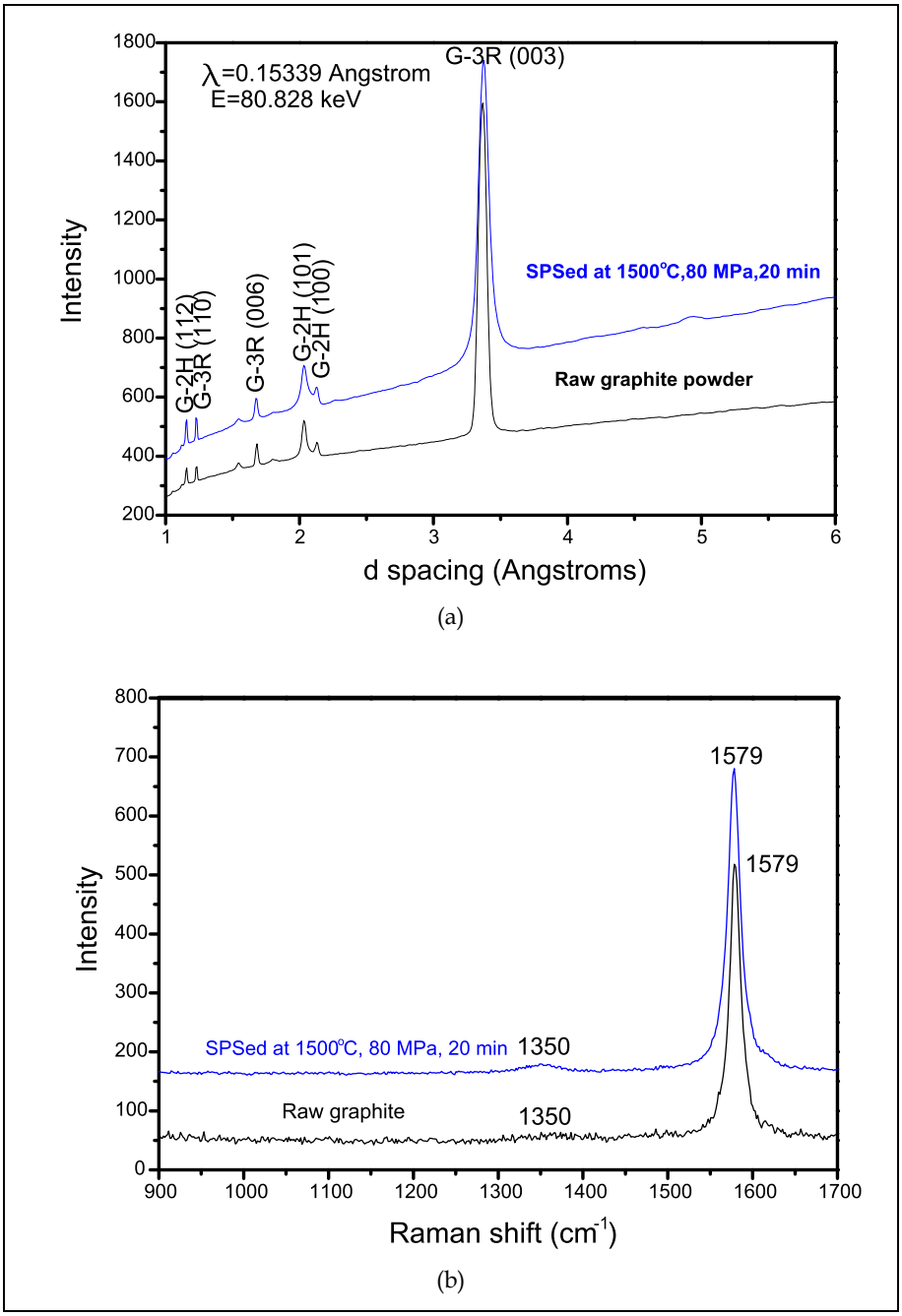

Fig. 5. Synchrotron radiation-high energy X-ray diffraction patterns (a) and Raman spectra (b) of the raw graphite and the spark plasma sintered graphite at 1500 ◦C, 80 MPa for 20 min.

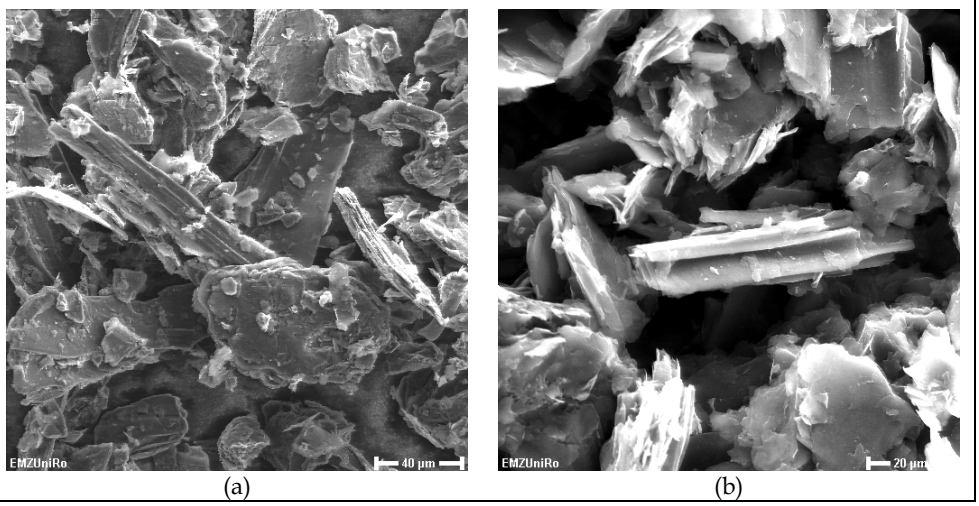

(a) (b)

Fig. 6. SEM micrographs of the raw graphite (a) and the spark plasma sintered graphite at 1500 °C, 80 MPa for 20 min (b).

under 80 MPa in a non-oxygen atmosphere during the AC sintering. Figure 7 (b) shows the synchrotron radiation-in situ X-ray diffraction patterns of the pure C60 at 80 MPa under different temperatures. There is no diamond formation in the C60 sample. It shows that the C60 is stable below the temperature of 900 °C. However, the C60 is unstable above that temperature point. The C60 (110) peak disappeared above temperature of 900 °C and C60 (112) peak disappeared above temperature of 990 °C. It is found that the graphite is very stable in the in-situ high temperature X-ray experiments at or below 1500 °C under 80 MPa.

3.3 Mechanisms

Synchrotron radiation-high energy X-ray diffraction was used to identify the diamond phase in the carbon samples after SPS. In order to confirm the diamond formation, Raman spectroscopy was also used to identify the formation of sp^3 bonded diamonds. By using the high energy X-ray diffraction and Raman spectroscopy, the cubic diamond phases were identified and confirmed in the SPSed MWCNTs and C60 samples. The n-diamond was also found in the SPSed MWCNTs sample. The n-diamond is a new kind of carbon allotrope, which is a metallic form of carbon with face-centred cubic structure. It is a metastable and intermediate phase, can decompose slowly at room temperature, and has been synthesized accidentally by various processes (Zhang, Mihoc et al., 2011). It is noted that the n-diamond can also be synthesized by the SPS process. The standard d spacings of the cubic diamond (111), (220) and (311) planes are centered at 2.059 Å, 1.261 Å and 1.075 Å (ICDD No. 65-537). The cubic diamond in the SPSed MWCNTs centered at 2.05, 1.23 and 1.06 Å, and in the SPSed C60 appeared at 2.06 and 1.23 Å spacing. The diffraction peaks of the synthesized diamond from MWCNTs and C60 are very close to the standard diamond diffraction data, but there is a little shift. The diamond peak shifts are due to the existence of residual stress

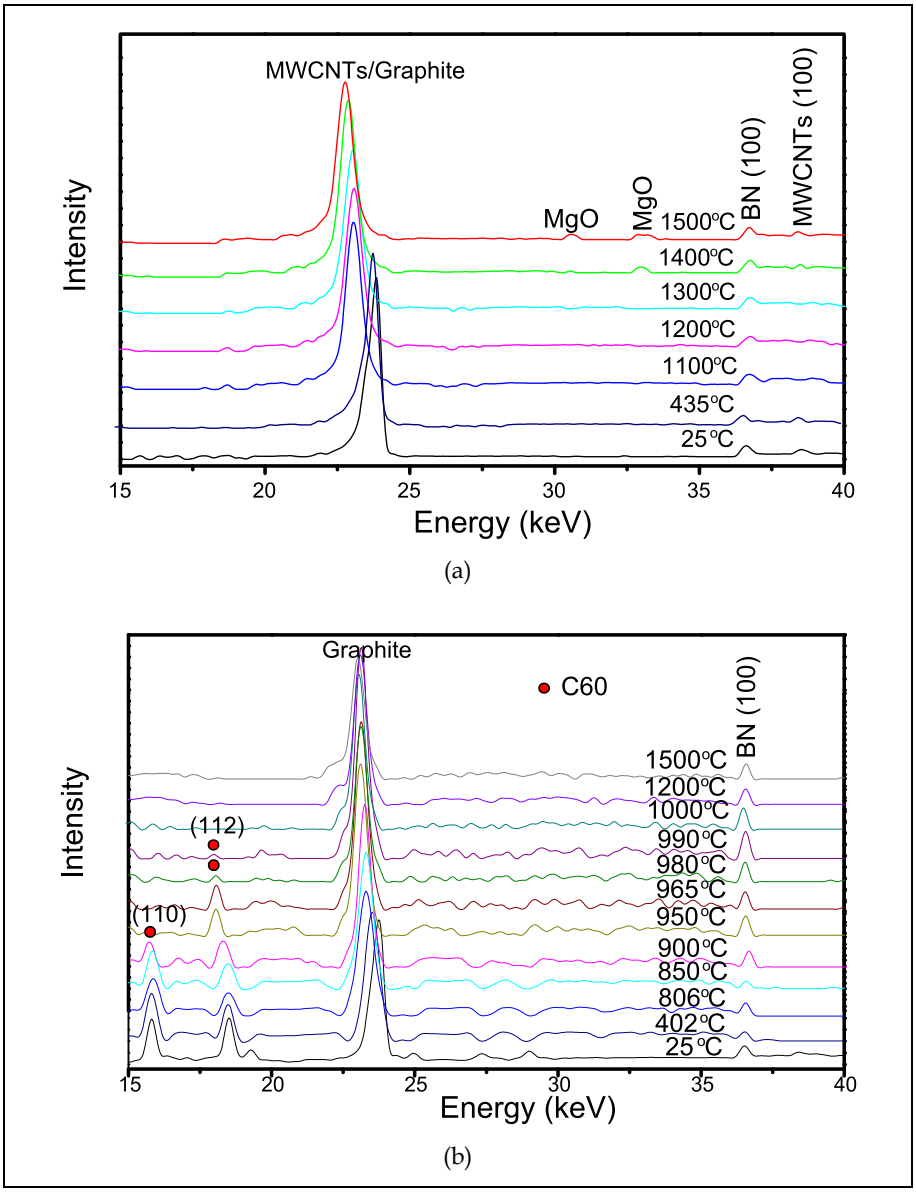

Fig. 7. Synchrotron radiation-in situ X-ray diffraction patterns of the pure MWCNTs (a) and C60 (b) at 80 MPa under different temperatures.

in the synthesized diamonds from MWCNTs and C60 by using the SPS. The residual stress of the diamond is because of the stress that remains after the original cause of the stresses (uniaxial forces, heat gradient) has been removed after the SPS processing. In this study, an uniaxial force of 80 MPa was applied and there generally existed some temperature

gradients during the operation of the SPS. Therefore, the diamond peaks in the SPSed MWCNTs and C60 have shifted a little. Combining the results of the Raman spectroscopy, the formation of diamond phases in these MWCNTs and C60 samples is confirmed. It is found that there are no C60 peaks in the X-ray diffraction and Raman results of the SPSed C60 sample, but there are strong unreacted MWCNTs peaks in the SPSed MWCNTs sample, and there are no diamond phases in the SPSed graphite sample. There exists a high activation barrier from the graphite, MWCNTs and C60 to diamond, the exact height of which is unknown. The results this study indicate that the activation barrier between the C60 and diamond is lower than that of the MWCNTs with diamond, and the barrier between MWCNTs and diamond is lower than that of the graphite with diamond. The graphite is the most stable crystalline modification of carbon among the MWCNTs, C60 and graphite allotropes under the SPS processing.

The SPS is a remarkable technique to synthesize and consolidate a large variety of materials. The process typically uses moderate uniaxial pressures usually below 100 MPa in combination with a pulsing on-off DC current during its operation. There are many mechanisms proposed to account for the enhanced sintering abilities of the SPS process; for example, field assisted diffusion, spark impact pressure, plasma cleaning of particle surfaces, Joule's heating, local melting and evaporation especially in metallic systems, surface activation on particles and electron wind force (Zhang, Mihoc et al., 2011). The one that draws the most controversy of these mechanisms involves the presence of momentary plasma. In this study, the diamond converted from the MWCNTs and C60 without any catalysts being involved in the SPS. However, the parallel investigations by using the synchrotron radiation in-situ high temperature X-ray diffraction show that there is no diamond formation in the MWCNTs and C60 samples in the AC sintering at the same pressure (80 MPa) and temperature (1500 ^{o}C). What is the phase transition mechanism from MWCNTs and C60 to diamond in the SPS? Such a clear, significant difference in the products is due to the special sintering principle of SPS. It is a field activated sintering technique based on an DC electric spark discharge phenomenon, i.e. a high energy and low voltage spark pulse DC momentarily generates sparking plasma between particles, which causes localized high temperatures. It is an electric AC heating in the in-situ high temperature experiments. Without plasma effect, it would need 8000-10000 ^{o}C at pressure of 80 MPa to get diamond from the MWCNTs and C60, as we calculated. Therefore, super-high pressures (5-10 GPa) are required for the diamond formation in the hydrostatic HPHT technique. Since the SPS only needs MPa level pressure, it is believed that the plasma plays the key role for the diamond transformation from the MWCNTs and C60. The high current, low voltage, momentary pulsed plasma discharge have generated highly localized Joule's heating up to a few thousand degrees Celsius between particles in few minutes. The current density in the SPS is typically on the order of 10^2 A/cm^2 and is highly concentrated at the inter-granular contact or interface (Yang et al., 2010). The momentary pulsed plasma provided energy equivalent to thousand degrees to help the nano-carbon across their activation barriers to the diamond phase. It leads to the transformation of mainly sp^2 bonded MWCNTs and C60 to sp^3 bonded diamonds. Despite the on-going argument about whether the spark plasmas actually occur during the SPS process, our present study, regarding generating diamond under such a low pressure, suggests that such spark plasmas indeed take place during SPS of these nano-carbon materials with excellent electrical conductivities and high surface areas. The plasmas generated very high localized temperatures up to about 8000-10000 ^{o}C and dramatically reduced the pressures required

for diamond formation from the GPa to the MPa level. Eventually, this research provided some new indirect evidences for the presence of plasmas during the SPS operation. Therefore, we take plasma into consideration in the thermodynamic analysis (Zhang, 2005; Zhang, Mihoc et al., 2010). The total energy for the diamond formation:

$$Q = \Delta H_T + Q_P + \Delta H_M ,$$

where Q is Total Energy, ΔH_T is the Energy due to temperature difference, Q_p is the Energy due to pressure difference, ΔH_M is the Energy due to plasma effect. The enthalpy of plasma:

$$H = H_E + H_K + H_D + H_I ,$$

where H is the plasma contribution, H_E is the kinetic contribution, H_K is the excitation contribution, H_D is the dissolution contribution, H_I is the electrolytic contribution. Then,

$$dS = \frac{\delta Q}{T} ,$$

$$\Delta Q(T) - \Delta Q(T_0) = \Delta S(T_0 - T) ,$$

Where T is the temperature, T_0 is the starting temperature, ΔQ is the difference of mol free energy, ΔS *is* the difference of mol entropy. Only when $\Delta Q(T)<0$, MWCNTs and C60 can be transformed into diamond. So, we can get an equation:

$$T > T_0 + \frac{\Delta Q(T_0)}{\Delta S}$$

The effect of the plasmas in the SPS has increased the entropy ΔS of the whole SPS system resulting in a lower sintering temperature T for the diamond formation. Diamond were converted from MWCNTs and C60 at 1500 °C under very low pressure of 80 MPa. The SPS is a marvelous process to prepare a wide range of advanced materials. The technique significantly uses uniaxial pressures normally 30-100 MPa to integrate a on-off DC current while its running. In this study, the diamond conversion in the SPSed MWCNTs and C60 samples without any catalysts being involved has validated the high localized temperatures between particles. This is due to the presence of momentary plasmas during SPS of these electrically conductive and high surface area nano-carbon materials. The plasmas have increased the entropy of the whole SPS system resulting in milder conditions for the diamond formation.

In summary, the thermal stability of MWCNTs, C60 and graphite has been investigated under the pulsed DC field in a SPS furnace. Cubic diamond and n-diamond have been converted from pure MWCNTs; cubic diamond has been converted from pure C60, both without catalysts being involved by the SPS at conditions of 1500 °C, 80 MPa for 20 min. There was no notice of diamond formation in the case of pure graphite sample processed by SPS at this condition. The graphite is the most stable crystalline modification of carbon among the MWCNTs, C60 and graphite allotropes under the SPS. The parallel investigations by using the synchrotron radiation in-situ high temperature (AC field) X-ray diffraction show that there is no diamond formation in the MWCNTs and C60 samples at the same pressure (80 MPa) and temperature (1500 °C). Their phase transitional mechanism from MWCNTs and C60 to diamond indicated the high localized temperatures between particles due to the presence of

momentary plasmas during the SPS process. The plasmas have increased the entropy of the SPS system resulted in milder conditions for the diamond formation.

4. Diamond synthesis with catalysts by the SPS

In the HPHT method, the involved solvent catalysts could decrease the energy barrier and affect the rate of a kinetics reaction for diamond nucleation and contribute to the formation of diamond from graphite. Besides being able to reduce the transforming temperature and pressure from graphite to diamond, they can also affect the quality and crystal form of the diamond (Zhang, Adam et al., 2011). It is indicated that the solvent catalysts may have the same effects to promote diamond growth from MWCNTs and graphite in the SPS method In this part, the catalysts were involved in the SPS diamond synthesis with carbon modifications of MWCNTs and graphite and the effects of catalysts were investigated.

4.1 Carbon nanotubes with FeNi catalyst

Currently preferred metal catalyst materials are Fe-Ni alloys, such as Fe-35Ni, Fe-31Ni-5Co, Fe-30Ni, and other INVAR alloys, where Fe-35Ni being the most preferred and more readily available (Zhang, Adam et al., 2011). In order to increase the transitional rate of diamond, the Fe35Ni alloy powders were chosen as catalysts for diamond synthesis from MWCNTs by the SPS method here. The starting MWCNTs materials have an external and internal diameter of ca. 40 nm and 20 nm, respectively. The MWCNTs/FeNi samples were sintered in the SPS furnace at various temperatures under 70 MPa for 20 min.

Figure 8 (a) shows the Raman spectra of the starting MWCNTs and the spark plasma sintered MWCNTs/Fe35Ni samples at 1100-1500 ^{o}C before etching. The diamond band (D band) of the starting MWCNTs appeared at 1345 cm^{-1}. After spark plasma sintering at 1100 ^{o}C, the D band has shifted to 1342 cm^{-1}. It was found that the characteristic Raman shift of the cubic diamond phase appeared at 1333 cm^{-1} in the 1200-1500 ^{o}C sintered samples. The D band shifted from the starting 1345 cm^{-1} to 1333 cm^{-1} indicating the diamond formation above temperatures of 1200 ^{o}C. The broad peak of Raman spectra at 1333 cm^{-1} in the 1200-1500 ^{o}C sintered samples is due to the existence of un-reacted MWCNTs. The G band is due to the E_{2g} mode of graphite band (G band), relating to the sp^2 bonded carbon vibrations in a 2-dimensional graphitic hexagonal lattice. The G bands appeared at 1570 cm^{-1} in the starting MWCNTs and 1100 ^{o}C sintered sample, has shifted to 1574 cm^{-1} (1200 ^{o}C), 1572 cm^{-1} (1300 ^{o}C), 1576 cm^{-1} (1400 ^{o}C), 1561 cm^{-1} (1500 ^{o}C), which implied the vibrations of sp^2 bonded carbon during the SPS. The Raman results indicated that diamonds are converted from the MWCNTs/Fe35Ni at temperatures of 1200-1500 ^{o}C.

Additionally, all the samples were etched in boiling acid to remove the FeNi catalysts and the un-reacted MWCNTs. Figure 8(b) shows the X-ray diffraction patterns of the starting MWCNTs, Fe35Ni catalyst, and the spark plasma sintered MWCNTs/Fe35Ni samples at 1100-1500 ^{o}C after etching with a CuKα radiation Bruker-XRD. The starting MWCNTs show the (002) plane at 2θ of 25.86 degree without Ni and La catalysts peaks. The Fe35Ni catalysts show diffraction peaks at 2θ of 43.60 and 50.79 degree. After etching of the obtained MWCNTs/Fe35Ni samples, no obvious Fe35Ni diffraction peaks were detected in the 1100-1500 ^{o}C sintered samples. It indicated that the FeNi catalysts have been completely removed from the carbon samples by the boiling acid treatment. The peak at 2θ of 42.90 degree in the raw CNTs has shifted to 43.37 degree in the 1100 ^{o}C sintered sample.

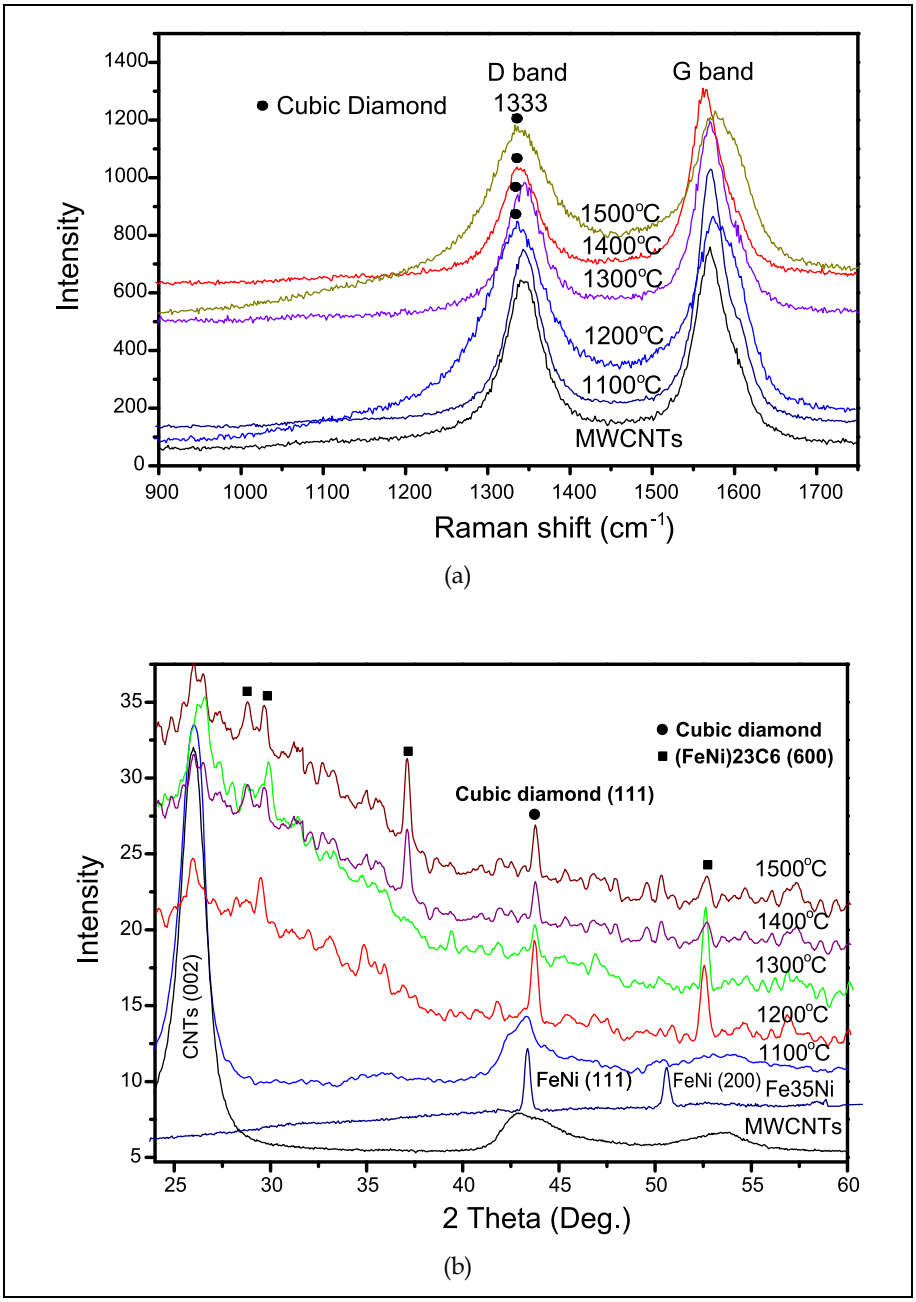

Fig. 8. Raman spectra of the starting MWCNTs and the spark plasma sintered MWCNTs/Fe35Ni samples at 1100-1500 °C before etching (a), and X-ray diffraction patterns of the starting MWCNTs, Fe35Ni catalyst, and the sintered samples after etching.

It is noted that this sample is in the transitional stage from CNTs to diamond. It is identified that the cubic diamond peak at 2θ of 43.95 with d spacing of 0.26 nm in the samples of 1200-1500 °C. There is still a broad CNTs (002) peak indicating there are some un-reacted and un-removed CNTs in the samples. Additionally, haxonite $(Fe,Ni)_{23}C_6$ peaks are found in the XRD results of 1200-1500 °C. With temperature increase from 1200 to 1500 °C, the haxonite peaks get stronger and stronger. This is due to the reaction between the FeNi catalysts and the MWCNTs at high temperatures. The Raman and XRD results confirmed the diamond formation in the 1200-1500 °C sintered samples.

The SEM micrographs of the spark plasma sintered MWCNTs/FeNi samples at 1100 °C and 1200 °C after etching are shown in Figure 9. Compared with the starting CNTs, the MWCNTs in the 1100 °C sample were almost melted and adhered together, but the tubular structure of the CNTs is noticeable in the growing diamond (Figure 9a). After sintered at 1200 °C, diamond crystals with sizes of 10-40 μm are observed in the samples (Figure 9b). These diamond crystals are in shape of hexahedron. Some flake-like carbons are noticed in the sample, as indicated by circles. The higher magnification SEM micrograph shows that the diamond crystals without residual CNTs left on their surface (Figure 9c). The high magnification micrograph in Figure 9 (d) indicated the layer-by-layer texture on the diamond crystals. The SEM micrographs of the spark plasma sintered MWCNTs/FeNi samples from 1300 °C to 1500 °C after etching were also studied (Zhang, Adam et al., 2011).. The particle size of the diamond crystals did not increase with the increase of sintering temperatures. A 1500 °C synthesized diamond with crystal size about 20 μm also showed clear layer-by-layer textures. On the matrix of this diamond crystal, there are many flake-like carbons. Such flake-like carbons were found in all these samples from 1300 to 1500 °C. The carbon flakes in these higher temperature sintered samples are similar to those in the 1200 °C sintered one. These flakes also showed layer-by-layer microstructures. The SEM observations agree well with the Raman and XRD results.

Figure 10 shows the TEM micrographs and selected area diffraction patterns of the spark plasma sintered MWCNTs/Fe35Ni sample at 1200 °C after etching. There are some mono-crystal and poly-crystal diamonds in the samples (Figure 10a-d). The monocrystalline diamond also shows the layer-by-layer structures (Figure 10a), which is consistent with the results of the SEM. The selected area diffraction pattern of the crystal in the bottom of the Figure 10 (a) confirmed the diamond is mono-crystal along [110] direction (Figure 10b). The poly-crystal diamond is in size of tens of micrometers (Figure 10c). The selected area diffraction pattern with diffraction rings were calculated and confirmed the diamonds are cubic poly-crystals (Figure 10d). The Raman, XRD, SEM, and TEM identification results have confirmed the diamond formation in MWCNTs with Fe35Ni as catalysts at a lower temperature of 1200 °C.

The Raman, XRD, SEM and TEM results confirmed that monocrystalline and polycrystalline diamonds were synthesized in the MWCNTs/Fe35Ni sample after SPS at temperatures above 1200 °C. The SEM results showed better diamond crystal shapes in the 1200 °C sintered samples. The TEM with selected area diffraction patterns showed the existence of diamond mono-crystals and poly-crystals in the 1200 °C sintered samples. Higher temperatures (1300-1500 °C) did not lead to larger diamond crystals as seen in the SEM images. The temperature 1200 °C is the optimal SPS temperature for the MWCNTs/Fe35Ni samples. This temperature 1200 °C for the diamond synthesis is much lower than that of the MWCNTs without catalyst (1500 °C) in our previous research (Zhang, Shen et al., 2005).

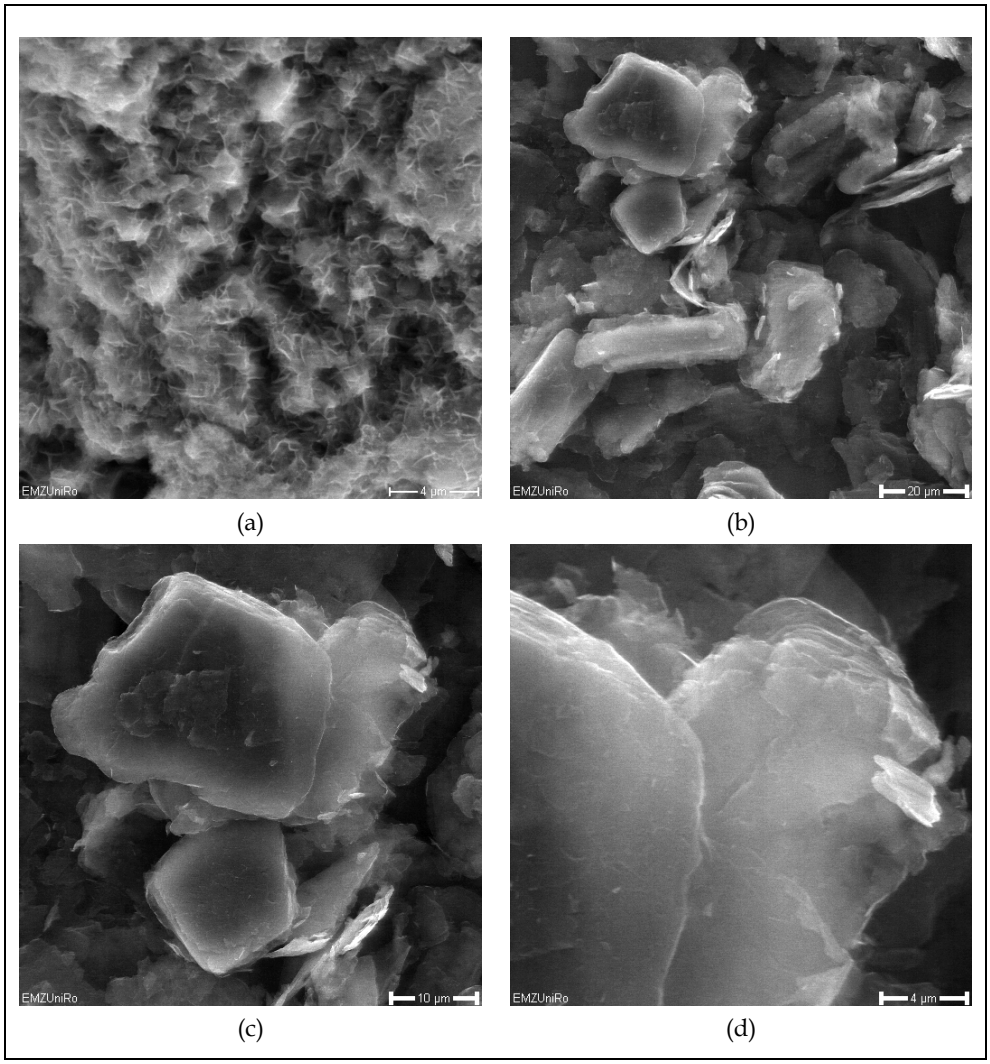

Fig. 9. SEM micrographs of the spark plasma sintered MWCNTs/Fe35Ni samples at 1100 °C (a), 1200 °C (b-d) after etching, exhibiting the growing process of diamond.

It indicates that the FeNi catalysts are effective to enhance the diamond conversion from MWCNTs in the SPS technique. The melting point of Fe35Ni alloy is about 1460 °C as measured in its phase diagram. During the SPS processing, the melting point of this Fe35Ni powder has been decreased due to the pulsed current induced powder activation, and the applied pressures. There is usually some temperature difference between the mold surface and the actual temperature in the SPS sample. The temperature measurement design in the FCT spark plasma sintering system allowed a very accurate temperature control since the temperature difference between the centre of the sample and the controlling pyrometer was

always below 5 °C (Vanmeensel et al., 2005). The catalysts of Fe35Ni alloy powders were melted at SPS temperature of 1200 °C, which was noticed during the SPS of the MWCNTs/Fe35Ni sample ; so that, it reduced the SPS temperature to 1200 °C and the pressure to 70 MPa for the diamond synthesis as well as increased the diamond transition rate using the MWCNTs as carbon sources. In general, milder conditions were realized for the diamond synthesis by using the Fe35Ni catalysts in this study. In the HPHT method, the carbon-carbon diagram for the diamond synthesis is crucial (Novikov, 1999). In this SPS method, there will be a new carbon-carbon diagram for the diamond synthesis, which can predict the optimal temperature, pressure regions for the diamond synthesis in this SPS method.

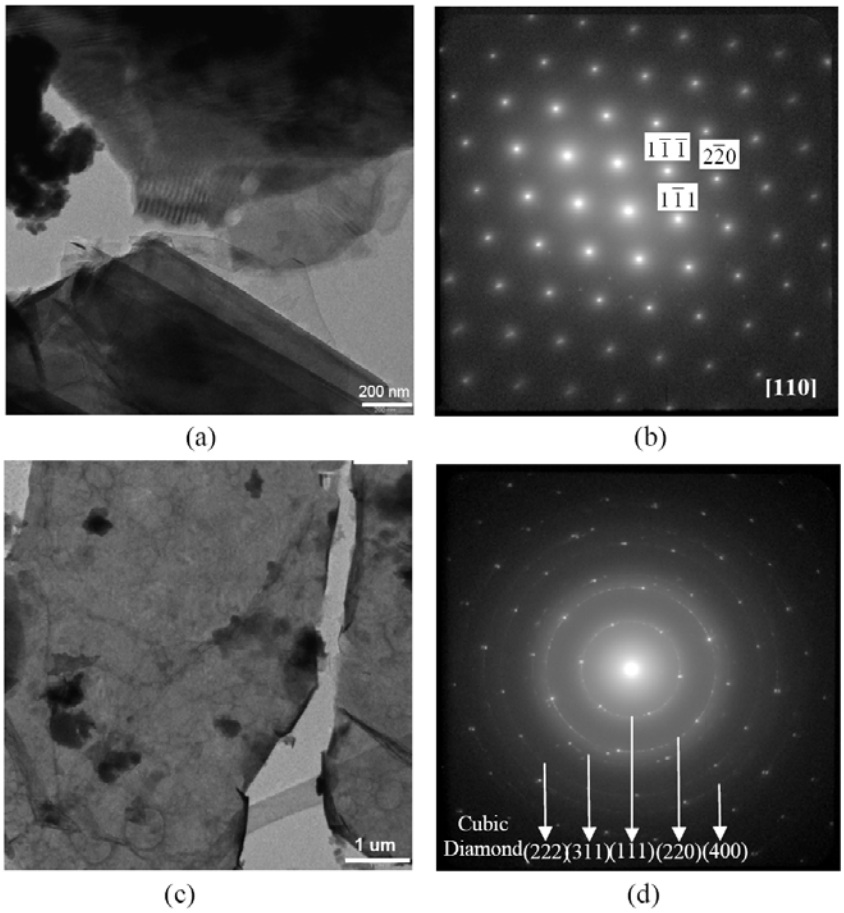

Fig. 10. TEM micrographs with selected area diffraction patterns (SADP) of the 1200 °C spark plasma sintered MWCNTs/Fe35Ni sample after etching, showing the monocrystalline diamond (a, b) and polycrystalline diamond (c, d).

A layer-by-layer structure of diamond crystals was found in the SEM and TEM micrographs. Our previous research revealed the initial diamond growth mechanism from MWCNTs to diamond in SPS without catalysts, that is from CNTs to intermediate phase carbon onions and finally to diamond. The diamond crystals in the samples without FeNi catalysts also show the similar layer-by-layer structures. Many flake-carbons with layers structures were found in the samples of 1200-1500 ^{o}C. These indicate that the diamonds were grown up from these carbon flakes. Based on the above analysis, a model for the growth of diamond crystals during the SPS is proposed in Figure 11. The direction of pressure during the SPS is in two axial directions, but not in six directions as the HPHT six-anvil press. Therefore, the diamonds were easier to growth in the direction without pressure. As a result, the MWCNTs were grown to layered diamond flakes vertically to the direction of pressure. Finally, several diamond flakes reacted together and formed a three-dimensional diamond crystal. The growth mechanism of diamond from MWCNTs is a layer-by-layer growth model in the SPS method. This model is available for the MWCNTs to diamond with and without catalysts. This mechanism will be constructive and helpful for the large diamond crystals synthesis by using the SPS technique.

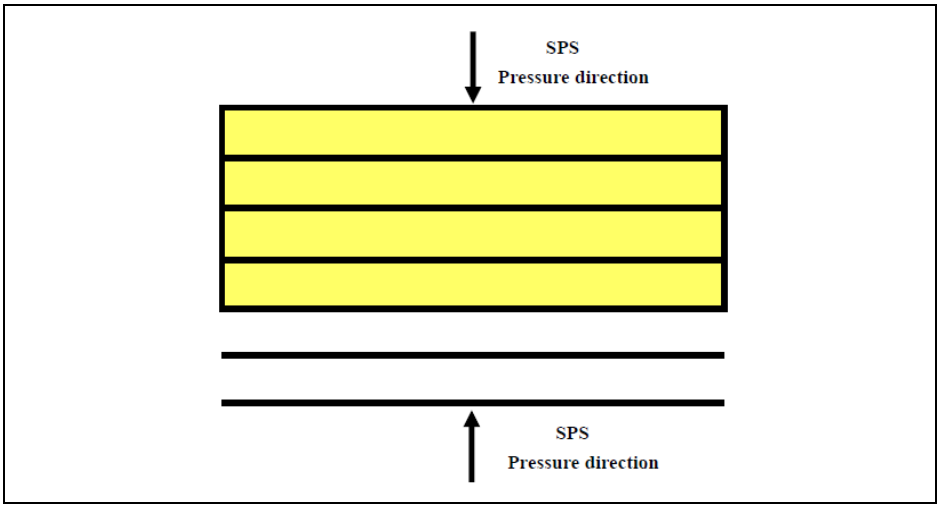

Fig. 11. Schematic illustration of the growth model of diamond crystals from MWCNTs in SPS.

In summary, a Fe35Ni solvent catalyst has been involved to synthesize diamond from MWCNTs by using the SPS technique. Cubic diamond crystals were synthesized from the MWCNTs/Fe35Ni mixtures at lower SPS temperature of 1200 ^{o}C under pressure of 70 MPa. In the sample, well-crystallized diamond mono-crystals and poly-crystals consisted particle sizes ranged 10-40 μm. The Fe35Ni catalysts achieved an effective reduction of the SPS temperature to 1200 ^{o}C and the SPS pressure to 70 MPa for the diamond synthesis, as well as an increment of diamond transition rate from MWCNTs in the SPS. A model was also proposed to describe the diamond growth and revealed as a layer-by-layer growth mechanism.

4.2 Graphite with various catalysts

Graphite has been used as the main carbon source for the diamond synthesis in the HPHT technique. In this study, the Ni, MnNi, MnNiFe and AlCuFe quasicrystal powder were tested as the catalysts for the diamond synthesis from the graphite by the SPS technique. Each catalyst was weighted and mixed with the graphite powder in the mass ratio of 4:6. The mixture powders were mixed homogeneously by high energy ball milling for 5 hours.

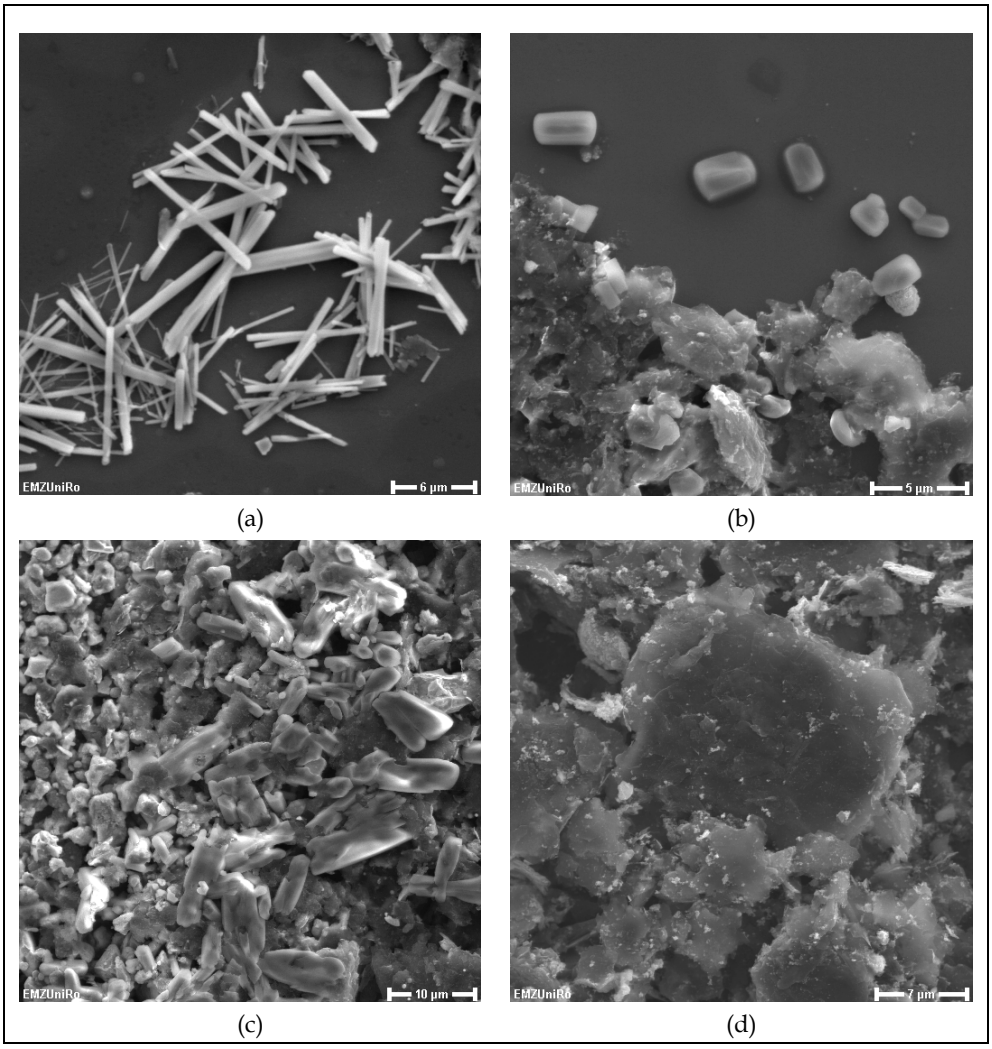

Fig. 12. SEM micrographs of the spark plasma sintered graphite samples at 1300 °C under 50 MPa with Ni (a), AlCuFe quasicrystal (b), MnNi (c), and MnNiFe powder catalysts (d) exhibiting the different diamonds.

Then, the mixtures were subjected to the SPS machine. The sintered samples were tested at SPS temperatures of 1200-1500 °C and under pressures of 10-80 MPa. The results show that diamond crystals can be converted from graphite at the SPS temperature of 1300 °C for holding time of 20 min under the pressure of 50 MPa.

Figure 12 shows the SEM micrographs of the spark plasma sintered graphite samples at 1300 °C for 20 min under 50 MPa with Ni, AlCuFe quasicrystal, MnNi, and MnNiFe powder catalysts after etching. It is interesting that we got diamond nano- and micro-rods with the Ni catalysts from the graphite (Figure 12a) by the SPS. The diameter of the diamond rods are from 80 nm to 2 μm. It is noted that the SPS also can be used as a new method to synthesize diamond nano- and micro-rods. The AlCuFe quasicrystal was introduced as catalyst for the graphite to diamond in the SPS. The diamond crystals with good diamond shapes from 1 to 3 μm were converted from the graphite with the AlCuFe catalyst. It indicates that the AlCuFe quasicrystal powder also can be used as catalyst for the conversion from graphite to diamond in the SPS. With MnNi catalysts, some short rod like diamond crystals are found in the sample (Figure 12c). However, in the sample of graphite/MnNiFe, there are no good diamond crystals visible (Figure 12d).

Additionally, the diamond phase was identified by the X-ray diffraction. Figure 13 shows the synchrotron radiation-high energy X-ray diffraction patterns of the spark plasma sintered graphite samples at 1300 °C under 50 MPa with Ni, AlCuFe quasicrystal , MnNi, and MnNiFe powder catalysts after etching. The Graphite/Ni sample shows strong cubic diamond peaks at d-spacing of 2.06, 1.26 and 1.07 Å. The Graphite/AlCuFe samples show

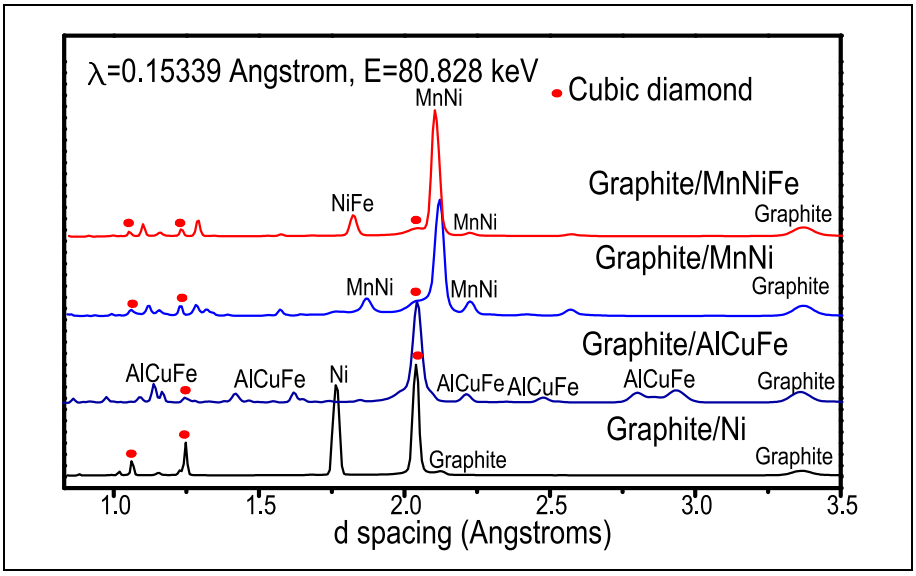

Fig. 13. Synchrotron radiation-high energy X-ray diffraction patterns of the spark plasma sintered graphite samples at 1300 °C under 50 MPa with Ni (a), AlCuFe quasicrystal (b), MnNi (c), and MnNiFe powder catalysts (d).

the strong diamond peaks at d-spacing of 2.06 and 1.26 Å. The Graphite/MnNi and Graphite/MnNiFe samples showed weak diamond peaks at d-spacing of 2.06, 1.26 and 1.07 Å. The XRD results agree well with the SEM results that good crystalline diamonds have been successfully synthesized from the graphite with catalysts of Ni and AlCuFe.

5. Factors affecting the diamond growth in the SPS

In this part, the factors that could affect the diamond growth will be studied in order to increase the diamond crystal size and transition rate. The factors including carbon modifications and atmospheres (Vacuum, Ar) will be studied and discussed.

5.1 Large diamond crystals from the C60 by the SPS

For the carbon modification selection, we will use the C60 as the carbon source for the diamond generation in the SPS. Our previous work has shown that C60 can be converted into diamond under the same SPS conditions as carbon nanotubes are converted to diamond (1500 oC, 80 MPa). Since the C60 has a higher sp^3 hybridization fraction than carbon nanotubes, it makes the transformation of C60 into diamond easier. Therefore, the C60 may be able to increase the diamond size in the SPS process. In this study, the diamond synthesis from the C60 was studied in the SPS (Zhang, Ahmed et al., 2011).

The C60 powders were spark plasma sintered (SPSed) at different temperatures under a pressure of 50 MPa. Figure 14 (a) shows the Raman spectra of the raw C60 and the SPSed C60 samples after etching. The raw C60 shows a sharp peak appeared at 1460 cm^{-1} and two weak broad peaks centered at 1568 and 1413 cm^{-1}. The cubic diamond peaks can also be detected at 1333 cm^{-1} in the Raman spectra taken for the samples processed in the temperature range from 1150 ^oC to 1500 ^oC under 50 MPa. However, the diamond band of the sample sintered at 1150 ^oC is very broad having the lowest height. Its graphite band at 1568 cm^{-1} is at the same value as that of the raw C60. It indicates that there is only a small fraction of diamond in this 1150 ^oC SPSed sample. With an increase in temperature to 1200 ^oC, 1300 ^oC and 1500 ^oC, the diamond band at 1333 cm^{-1} gets sharper and sharper, as well as the graphite band is shifted to a higher value of 1576 cm^{-1}. The result of the 1300 ^oC SPSed C60 shows the Raman spectra similar to the 1500 ^oC SPSed sample. Figure 14 (b) shows the XRD results of the raw C60 and the SPSed C60 samples after etching. In the 1150 ^oC sintered C60 sample, we found very weak diamond peaks. The C60 after SPS at temperatures above 1200 ^oC show the cubic diamond diffraction peaks at d spacing of 2.06 and 1.26 Å and a broad graphite peak. The C60 diffraction peaks disappeared indicate that the C60 has completely transformed into diamond and graphite phases after the SPS processing at temperatures from 1200-1500 ^oC.

The SEM micrographs of the C60 samples SPSed from 1150 to 1500 ^oC after etching are shown in Figure 15. There are few fine diamond crystals in the 1150 ^oC SPSed sample (Figure 15a). Some diamond crystals with hexagonal, tetragonal or triangular shapes are found in the micrograph of the 1200 ^oC SPSed sample (Figure 15b). The particle sizes of the diamond crystals are from tens of micrometers up to 200 μm. The diamond crystals with perfect hexahedron shapes are clearly observed in the 1300 ^oC sintered sample (Figure 15c). The diamond sizes range from 100 to 250 μm, they are larger than those of the sample sintered at 1200 ^oC. The SEM micrographs of the 1500 ^oC sintered C60 samples show that the big diamond crystals are almost melted. There are many small diamond crystals below 4 μm on big crystals.

It is obvious that the diamond crystal sizes do not increase with the increase in temperature; however, well-defined diamond crystals are created. A processing temperature of 1300 °C is the best for the phase transformation of C60 directly to diamond, according to this study.

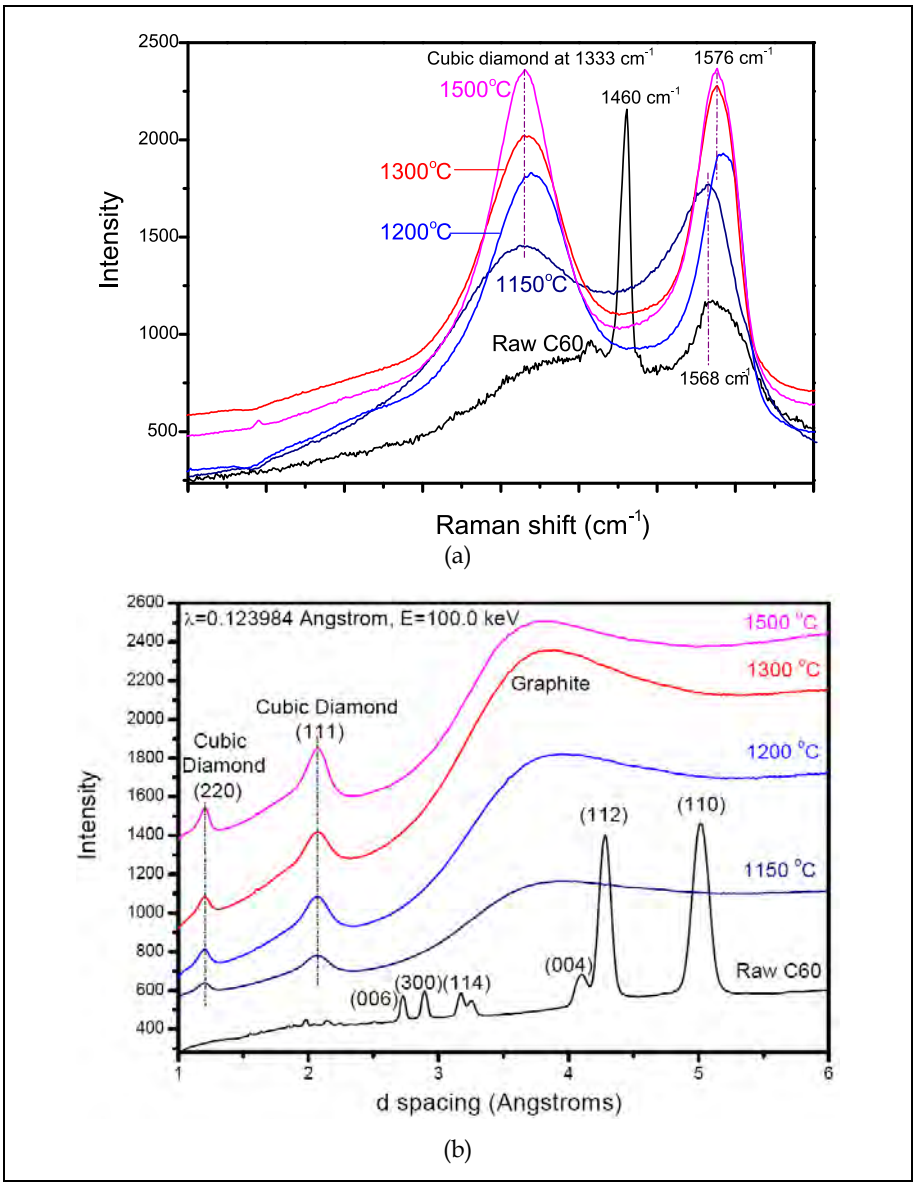

Fig. 14. Raman spectra (a) and Synchrotron radiation-high energy X-ray diffraction patterns (b) of the raw C60 and the spark plasma sintered C60 at different temperatures under 50 MPa pressure.

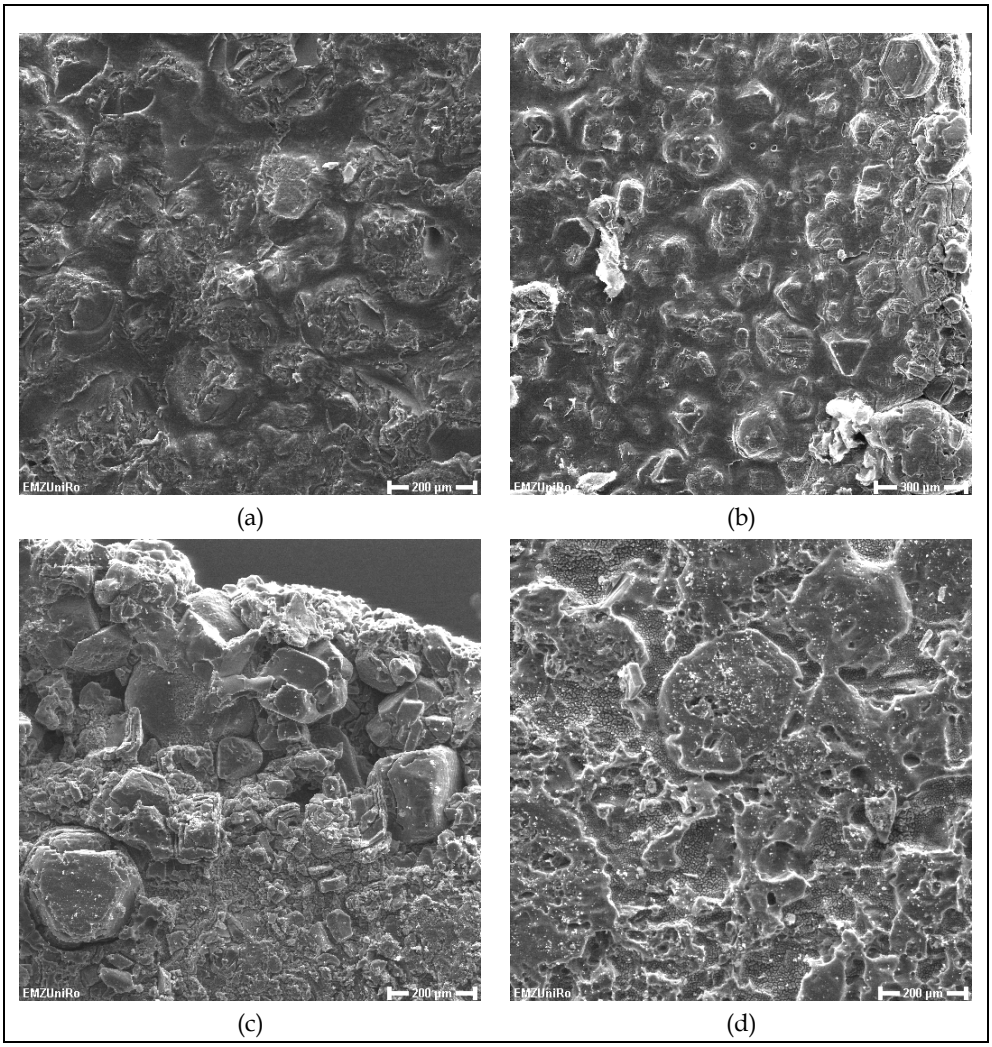

Fig. 15. SEM micrographs of spark plasma sintered C60 samples at 1150 °C(a), 1200 °C (b), 1300 °C (c), and 1500 °C (d) after etching, showing the diamond formation.

The particle size of the diamond crystals made from C60 is up to 250 µm. It is a very large size for such conversion without any catalyst being involved in the process. The carbon atoms in C60 are sp^2 hybridized with a high fraction of sp^3 hybridized structure due to angular strain. It is difficult to transform the planar sp^2 structure to the diamond sp^3 network. The C60 can be considered as a folded graphite sheet with the predominant hybridization sp^3 in the pentagons. This makes the transformation of C60 into diamond easier. A dense assembly of C60 spheroids, where 48 out of 60 carbon atoms have quasi-tetrahedral coordination, is sterically fairly close to that of the diamond (Regueiro et al., 1992). It implies that a small rearrangement of the atoms of C60 can result in the change of

its structure. However, it still needs solely superhigh pressure or high pressure and high temperatures for the phase transition from C60 to diamond (Zhang, Ahmed et al., 2011). We got diamond from C60 by the SPS at only 50 MPa and temperatures above 1150 °C. Well-crystallized diamonds with particle sizes up to 250 μm are obtained at 1300 °C and no further growth in particle size is seen beyond this temperature.

5.2 Effects of the CNTs diameters on the diamond sizes by the SPS

In the previous research, it was proposed that the CNTs transformed to carbon nano-onions, and the nucleation and growth of the diamond phase within the onion cores (Shen, Zhang et al., 2006). A model for the diamond nucleation at the internal surface of carbon onion was established, as shown in Fig.16. Based on this model, the energy need for the nucleation of diamond at the internal surface of carbon onion can be formulized (Zhang, 2005):

$$\Delta G = \Delta G_V + \Delta G_S + \Delta G_E$$

Where ΔG — Difference of Free energy for the nucleation of diamond；

ΔG_V — Difference of Volume Free energy for the nucleation of diamond；
ΔG_S — Difference of Surface Free energy for the nucleation of diamond；
ΔG_E — Difference of Elastic strain energy for the nucleation of diamond.

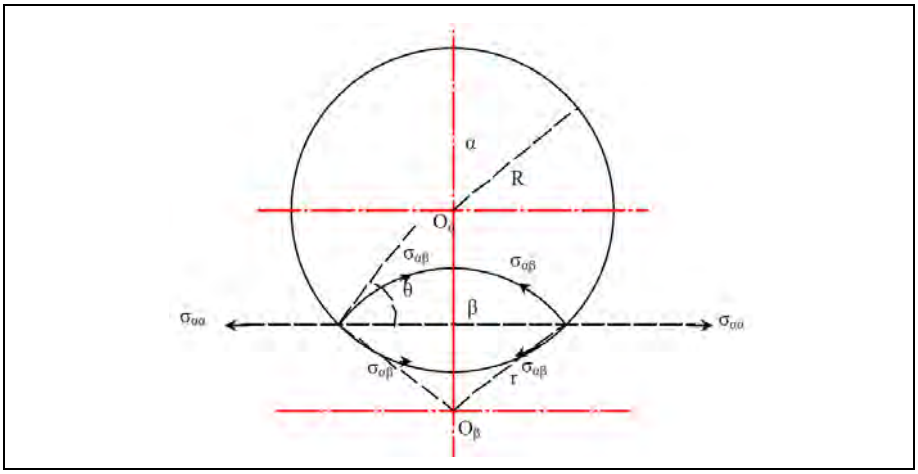

Fig. 16. Model for diamond (β) nucleation at the internal surface of carbon onion (α).

$$\Delta G_V = \frac{\pi \Delta g_V}{3}\left\{r^3\left(2-3\cos\theta+\cos^3\theta\right)+R^3\left(2-3\sin\theta+\sin^3\theta\right)\right\}$$

$$\Delta G_S = 2\pi\sigma_{\alpha\beta}\left\{r^2(1-\cos\theta)+R^2(1-\sin\theta)\right\}$$

$$\Delta G_E = V\Delta g_E = \Delta g_E\left\{\frac{\pi r^3}{3}\left(2-3\cos\theta+\cos^3\theta\right)+\frac{\pi R^3}{3}\left(2-3\sin\theta+\sin^3\theta\right)\right\}$$

Nuclear powder of diamond from carbon onion ΔG,

$$\Delta G = \left(\frac{\pi \Delta g_V}{3} + \Delta g_E\right)\left\{\begin{matrix} r^3\left(2 - 3\cos\theta + \cos^3\theta\right) + \\ R^3\left(2 - 3\sin\theta + \sin^3\theta\right) \end{matrix}\right\}$$
$$+2\pi\sigma_{\alpha\beta}\left\{r^2(1-\cos\theta) + R^2(1-\sin\theta)\right\}$$

The above equation shows the that decrease of R leads to the decrease of ΔG. The value of R is the inner radius of CNTs. It means the decrease of the diameter of CNTs could decrease the energy for the diamond nucleation ΔG. The lower ΔG leads to higher transition rates and larger particle sizes of diamond. This was validated by the following experiments.

The MWCNTs with diameters from 10-100nm were mixed with Fe35Ni catalyst at a weight ratio of 1:1 by ball milling, and pressed into a graphite die for SPS treatment (1200 °C, 50 MPa, 20 min) to form disk-shaped samples. The raw materials used in this experiment was shown in Table 1 with internal diameters of 10-20 nm, 20-40 nm, 40-60 nm and 60-100 nm.

Main range of diameter of MWCNTs	10-20 nm	20-40 nm	40-60 nm	60-100 nm
Length	5-15 μm	5-15 μm	5-15 μm	5-15 μm
Purity	>95%	>95%	>95%	>95%
Ash	<0.2 wt%	<0.2 wt%	<0.2 wt%	<0.2 wt%
Specific surface area	40-300 m^2/g	40-300 m^2/g	40-300 m^2/g	40-300 m^2/g
Amorphous carbon	<3%	<3%	<3%	<3%

Table 1. The raw materials those used in this experiments.

The SPSed samples after etching were subjected to the SEM analysis. Figure 17 shows the SEM micrographs of the diamond crystals obtained from different MWCNTs. It really shows various diamond sizes. The 10-20 nm MWCNTs generated 15-30 μm diamond crystals. The 20-40 nm MWCNTs generated 10-20 μm diamond. The 40-60 nm MWCNTs produced 7-10 μm diamonds, and the 60-100 nm MWCNTs formed 4-10 μm diamonds. The results are summarized in Table 2. It indicates that smaller diameters MWCNTs could produce larger diamond particles.

Main range of diameter of MWCNTs	10-20 nm	20-40 nm	40-60 nm	60-100 nm
Diamond particle size	15-30 μm	10-20 μm	7-15 μm	4-10 μm

Table 2. The diamond particle size from various MWCNTs.

The Raman results also confirmed the higher transition rate in the 10-20 nm MWCNTs. Therefore, the experiments validated the theoretical assumption. Consequently, the MWCNTs have been transformed into diamond under SPS conditions in presence of a FeNi catalyst at pressures of 50 MPa and temperatures of 1200 °C. The diamond particle size depends on the diameter of the MWCNTs. The MWCNTs with diameters from 60 to 100nm produced diamond particle from 4 to 10 μm, while in the sample of MWCNTs with diameters from 10 to 20 nm generated diamond particle sizes from 15 to 30 μm.

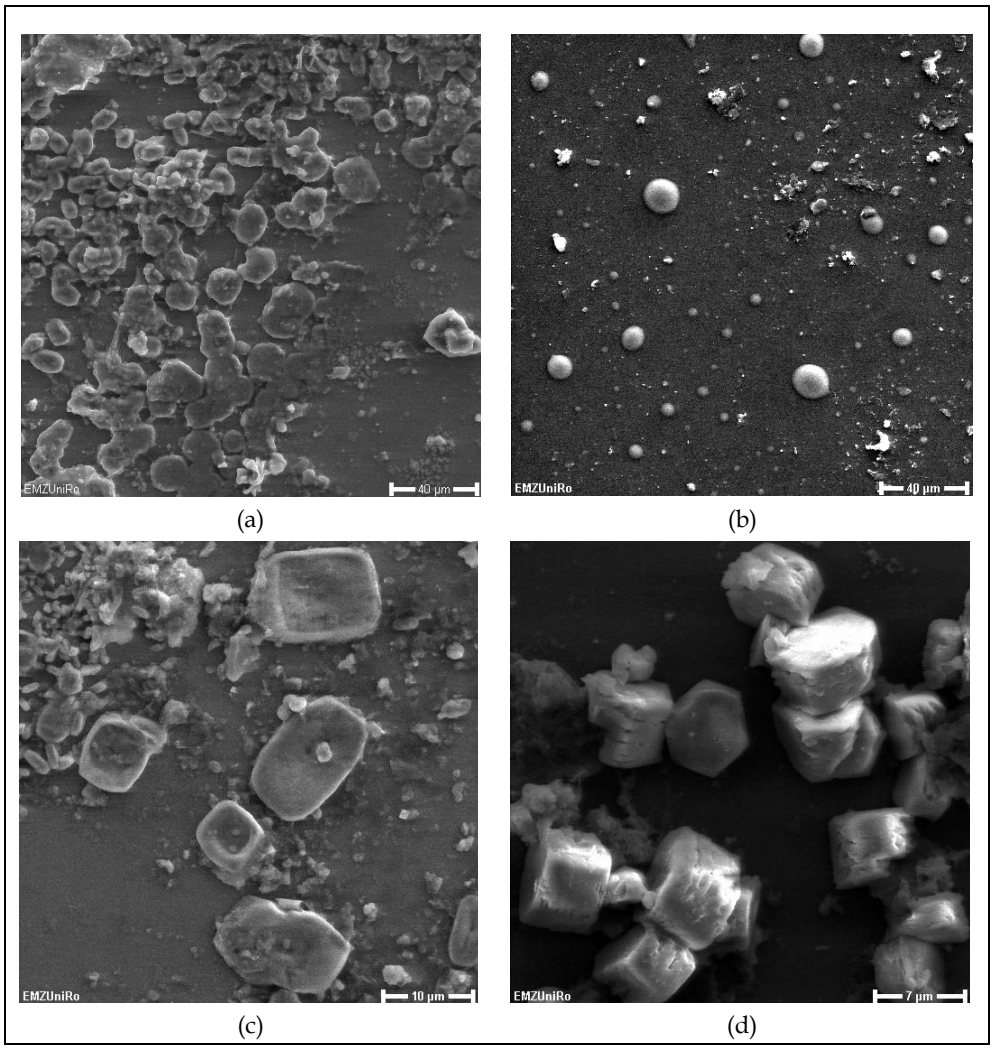

Fig. 17. SEM micrographs of the SPSed MWCNT/FeNi samples with various internal nanotube diameters of 10-20 nm (a), 20-40 nm (b), 40-60 nm (c) and 60-100 nm (d) showing the different diamond sizes.

5.3 Effect of atmospheres on the diamond growth in the SPS

In the SPS process, we usually use the vacuum atmosphere. We proposed that the plasma plays the key role for the diamond transition from various carbon modifications. Based on the theory of plasma physics, the gases like H_2, Ar, O_2, and so on can be used as plasma generating gases which can enhance the plasmas generation (Zheng et al., 2009). Therefore, in this study, the effect of the atmosphere on the diamond growth in the SPS was studied. The MWCNTs/FeNi mixture powders were spark plasma sintered in vacuum and Ar gas atmospheres at 1200 °C under 10 MPa which is the minimum pressure of the Model HP D-5 FCT SPS system. The sintered samples were etched and examined by the SEM and Raman spectroscopy.

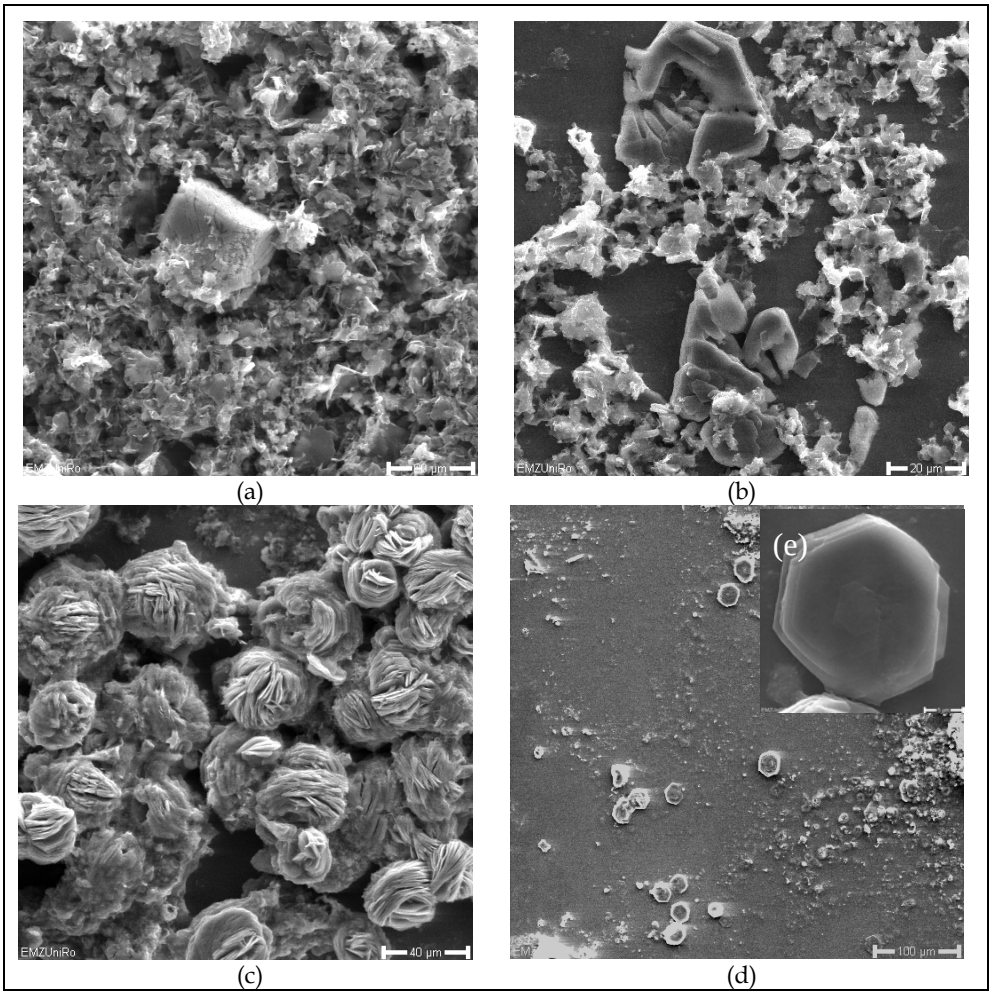

Fig. 18. SEM micrographs of the MWCNTs/FeNi samples SPSed at 1200 °C under 10 MPa in vacuum (a, b) and Ar gas (c-e).

Figure 18 shows the SEM micrographs of the MWCNTs/FeNi samples SPSed at 1200 °C under 10 MPa in vacuum and Ar gas. There are only a few poor quality diamond crystals created in the vacuum atmosphere of the SPS (Figure 18 a, b). In the case of the SPS treatment in Ar gas atmosphere, some flower-like structured carbon are observable (Figure 18c). This indicates that sparking plasmas may have happened and generated such flower-like structured carbon. It is exciting that some high quality diamond crystals with hexahedron structures are found in the sample (Figure 18 d). A high magnification SEM micrograph of one perfect diamond crystal is shown in Figure 18 (e).

Figure 19 shows the Raman spectra of the MWCNTs/FeNi samples SPSed at 1200 °C under 10 MPa in vacuum and Ar gas. Both of them show the cubic diamond peak at 1332 cm^{-1} Raman shift. The vacuum atmosphere SPSed sample shows a very weak diamond peak; however, the Ar gas atmosphere SPSed sample exhibits a strong diamond peak. Both of the G bands centered at the same Raman shift. But it is much sharper in the vacuum atmosphere SPSed sample than that in the Ar gas. The Raman results are accordingly to the SEM results that the Ar gas atmosphere in the SPS promotes the diamond formation. The SPS pressure that we used is very small (10 MPa), so that the pressure effect is negligible for the diamond conversion. The diamonds have been generated by the SPS from such low pressure in vacuum and Ar gas atmospheres. It means that the plasma played the key role for the diamond formation. It provided another evidence for the existence of plasma during the SPS that such a low pressure diamond formation. The Ar gas atmosphere enhanced plasma generation and promoted the diamond transition.

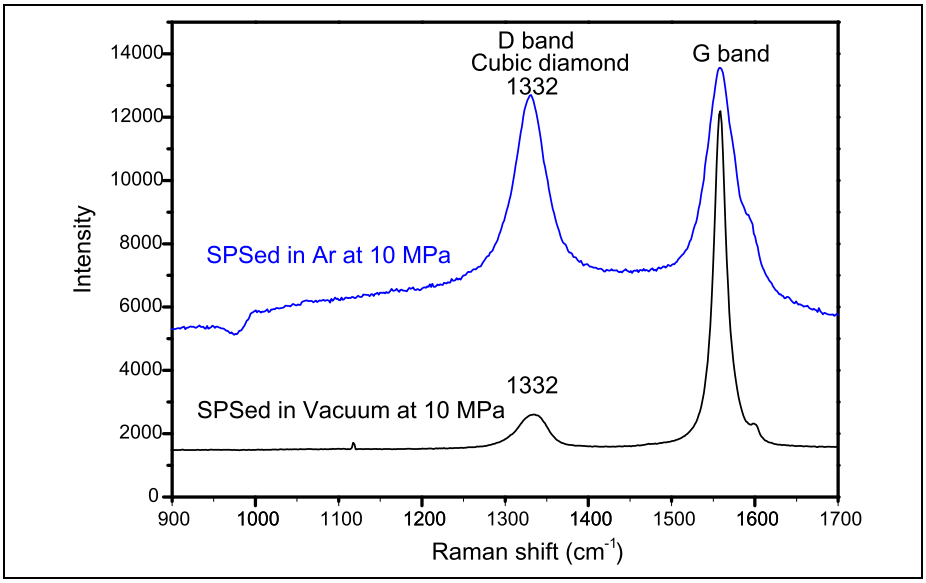

Fig. 19. Raman spectra of the MWCNTs/NiFe samples SPSed at 1200 °C in vacuum and Ar gas.

In this part, we investigated the factors affecting the diamond growth in the SPS. It is found that the C60 is able to increase the diamond size in the SPS process. Due to the high price of the C60, it is suggested that the C60 can be used as a doping catalyst material to promote the diamond transition. The diamond particle size depends on the internal diameter of the MWCNTs. Smaller diameter MWCNTs generated larger diamond particles. It is suggested to choose the smaller diameter MWCNTs when the MWCNTs are used as carbon source for the diamond synthesis in SPS. The Ar gas atmosphere enhanced plasma generation and promoted the diamond transition. It indicates that we select the Ar gas atmosphere to enhance the plasma effect in the SPS.

In this chapter, the diamond synthesis using the SPS was investigated and discussed. The diamond synthesis from pure carbon nanotubes has been covered by China Patent ZL 200410044157.0. (Shen, Zhang, 2004). The diamond synthesis from all the carbon modifications with catalysts as well as pure C60, graphene to diamond has been protected by the Deutsches Patent P162-11 (Zhang, Burkel et al. 2011). The SPS is a new technique for the diamond synthesis. It still needs further investigations to promote the SPS method to be used as a large-scale synthetic diamond production technique.

6. Conclusions and outlook

The thermal stability of MWCNTs, C60 and graphite has been investigated under the pulsed DC field in the SPS furnace. Cubic diamond and n-diamond have been converted from pure MWCNTs; cubic diamond has been converted from pure C60 without catalysts being involved by the SPS at conditions of 1500 ^{o}C and 80 MPa for 20 min. There was no notice of diamond formation in the case of pure graphite sample processed by SPS at this condition. The graphite is the most stable crystalline modification of carbon among the MWCNTs, C60 and graphite allotropes under the SPS. The parallel investigations by using the synchrotron radiation in-situ high temperature X-ray diffraction show that there is no diamond formation in the MWCNTs and C60 samples at the same pressure (80 MPa) and temperature (1500 ^{o}C). Their phase transition mechanisms from MWCNTs and C60 to diamond indicated the high localized temperatures between particles due to the presence of momentary plasmas during the SPS process. The thermal dynamic analysis reveals that the plasmas have increased the entropy of the SPS system resulting in milder conditions for the diamond formation.

Catalysts were involved in the SPS diamond synthesis with carbon modifications of carbon nanotubes and graphite. A Fe35Ni solvent catalyst has been incorporated to synthesize diamond from MWCNTs by using the SPS. Cubic diamond crystals were synthesized from the MWCNTs/Fe35Ni mixtures at lower SPS temperature of 1200 ^{o}C under pressure of 70 MPa. Well-crystallized diamond mono-crystals and poly-crystals with particle sizes ranging around 10-40 μm are synthesized. The Fe35Ni catalysts achieved an effective reduction of the SPS temperature to 1200 ^{o}C and the SPS pressure to 70 MPa for the diamond synthesis, as well as an increment of the diamond transition rate from MWCNTs in the SPS. A model was also proposed to describe the diamond growth and revealed as a layer-by-layer growth mechanism. The Ni, MnNi, MnNiFe and AlCuFe quasicrystal powder were used as the catalysts for the diamond synthesis from graphite by the SPS. Diamond crystals have been

converted from the graphite at the SPS condition of 1300 °C and 50 MPa for 20 min. Diamond nano- and micro-rods (80 nm-2 μm) have been obtained with the Ni catalysts from the graphite by the SPS. Diamond crystals with good diamond shapes from 1 to 3 μm have been converted from the graphite with the AlCuFe catalyst.

The factors affecting the diamond growth including carbon modifications and atmospheres have been studied in order to increase the diamond crystal size and transition rate. Well-crystallized diamonds with particle sizes up to 250 μm are obtained at 1300 °C by using the fullerene C60 as the carbon source. The mechanism analysis indicates that the high sp^3 hybrid fraction in the C60 leads to its transformation to diamond at lower pressures and temperature during the SPS application. It is suggested that the C60 can be used as doping catalyst materials to promote the diamond transition. A model for the diamond nucleation at the internal surface of carbon onion has been established. Based on the model, the energy need for the nucleation of diamond at the internal surface of carbon onion has been formulized. It is postulated that the decrease of diameter of CNTs could decrease the energy for the diamond nucleation. The results show that the MWCNTs with diameters from 60 to 100nm produced diamond particle from 4 to 10 μm, while in the sample of MWCNTs with diameters from 10 to 20 nm generated diamond particle sizes from 15 to 30 μm. The transition rate has been increased in the 10-20 nm MWCNTs. The experiments validated the theoretical assumption. The effect of the atmosphere on the diamond growth in the SPS was studied. The MWCNTs/FeNi mixture powders were spark plasma sintered in vacuum and Ar gas atmospheres at 1200 °C under the minimum pressure of 10 MPa. The diamonds have been generated by the SPS from such a low pressure in vacuum and Ar gas atmospheres. High quality diamond crystals with hexahedron structures are created in the Ar gas atmosphere of the SPS. It provided another evidence for the existence of plasma during the SPS because of such a low pressure diamond formation. The Ar gas atmosphere enhanced the plasma generation and promoted the diamond transition.

What makes the SPS so interesting for the diamond synthesis is the fact that only relatively low pressures of 10-80 MPa are needed. The SPS possesses a wide range of sintering temperatures from a few hundreds up to 2000 °C, controllable heating rates which can be set to several hundred degrees per minute for extremely rapid processing, as well as the capacity to process large samples up to 100 mm in diameter and 20 mm thick. As we know, the HPHT technique only can prepare very small samples in order to achieve the several GPa level high pressures. Therefore, the SPS is a highly efficient and energy saving technique for diamond synthesis. The investigation in this chapter indicate that the SPS, a pulsed electric field processing technique, has great potential to be used as an alternative and novel method for high-efficiency diamond generation. The diamond generation at such low pressures also provided some indirect evidences for the presence of plasmas during the SPS operation. However, it still needs further investigations to promote the SPS method to be used as a large-scale synthetic diamond production technique. The future highlights will be the development of diamond purification methods to get high purity diamond crystals from the SPSed carbon compacts and the synthesis of millimetre sized diamond crystals and achieving higher diamond transitional rate by using the SPS technique. The mechanical properties (hardness, Elastic modulus) and functional properties including electrical, thermal, optical, magnetic properties etc. of the SPSed diamond particles and the SPSed carbon samples with in-situ formed diamonds need to be investigated. The in-situ synthesis

of diamond/ceramics or diamond/metals composites from CNTs/ceramics or CNTs/metals by the SPS is also a very interesting subject for the future researches.

7. Acknowledgements

The authors acknowledge the financial support from the DFG-Deutschen Forschungsgemeinschaft (German Research Foundation) with grant No. BU 547/10-1 and the HASYLAB/DESY project with grant No. II-20090264. We also thank Dr. Christian Lathe, Dr. Martin von Zimmermann, Dr. Jozef Bednarcik at HASYLAB/DESY, Hamburg for their supports in the F2.1 and BW5 experiments, and Dr. Furqan Ahmed at the University of Erlangen-Nürnberg for his support in the Raman spectroscopy experiments.

8. References

Anselmi-Tamburini, U.; Gennari, S.; Garay, J. E.; Munir, Z. A. (2005). Fundamental investigations on the spark plasma sintering/synthesis process: II. Modeling of current and temperature distributions. *Mater. Sci. Eng. A.* 394: 139-148

Giardini, A. A.; Tydings, J. E.; Levin, S. B. (1960). A very high pressure-high temperature research apparatus and the synthesis of diamond. *American Mineralogist*. 45(1-2): 217-221

Hirose, Y.; Amanuma, S.; Komaki, K. (1990). The Synthesis of High-Quality Diamond in Combustion Flames. *Journal of Applied Physics*. 68(12):6401-6415

Hulbert, D. M.; Anders, A.; Dudina, D. V.; Andersson, J.; Jiang, D.; Unuvar, C.; Anselmi-Tamburini, U.; Lavernia, E. J.; Mukherjee, A. K. (2008). The absence of plasma in `spark plasma sintering'. *J. Appl. Phys.* 104(3): 033305-7

Kobashi, K.; Nishimura, K.; Kawate, Y.; Horiuchi T. (1988). Synthesis of diamonds by use of microwave plasma chemical-vapor deposition-morphology and growth of diamond Films. *Physical Review B*. 38(6):4067-4084

Novikov, N.V. (1999). New trends in high-pressure synthesis of diamond. *Diamond and Related Materials*. 8(8-9):1427-1432

Regueiro, M. N.; Monceau, P.; Hodeau, J.L. (1992). Crushing C60 to diamond at room temperature. *Nature.* 355: 237-239

Shen, J.; Zhang, F.; Sun J. F.; Wang, G. (2004). Low pressure synthesis of diamonds from carbon nanotubes by a new process. *China Patent.* ZL 200410044157.0

Shen, J.; Zhang, F.; Sun, J. F.; Zhu, Y. Q.; McCartney, D. G. (2006). Spark plasma sintering assisted diamond formation from carbon nanotubes at very low pressure. *Nanotechnology*. 17: 2187-2191

Vanmeensel, K.; Laptev, A.; Hennicke, J.; Vleugels, J.; Van der Biest, O. (2005). Modelling of the temperature distribution during field assisted sintering. *Acta Materialia*. 53: 4379-4388

Vereschagin, A. L.; Sakovich, G. V.; Komarov, V. F.; Petrov, E. A. (1994). Properties of ultrafine diamond clusters from detonation synthesis. *Diamond and Related Materials*. 3(1-2):160-162

Watanabe, I.; Matsushita, T.; Sasahara, K. (1992). Low-temperature synthesis of diamond films in thermoassisted Rf plasma chemical vapor-deposition. *Japanese Journal of Applied Physics Part 1.* 31(5A):1428-31

Yang, K.; He, J.; Su, Z.; Reppert, J. B.; Skove, M. J.; Tritt, T. M.; Rao, A. M. (2010). Inter-tube bonding, graphene formation and anisotropic transport properties in spark plasma sintered multi-wall carbon nanotube arrays. *Carbon*. 48:756-762

Zhang, F. (2005). Strengthening and toughening mechanisms of carbon nanotubes reinforced WC nanocomposites synthesized by spark plasma sintering. *Ph.D thesis*. Harbin Institute of Technology

Zhang, F., Shen, J.; Sun, J.; Zhu, Y. Q.; Wang, G.; McCartney, G. (2005). Conversion of carbon nanotubes to diamond by a spark plasma sintering. *Carbon*. 43:1254-1258

Zhang, F.; Shen, J.; Sun, J. F.; McCartney, D. G. (2006). Direct synthesis of diamond from low purity carbon nanotubes. *Carbon*. 44 : 3136-3138

Zhang, F.; Burkel. E. (2010). Novel titanium manganese alloys and their macroporous foams for biomedical applications prepared by field assisted sintering. In: *Biomedical Engineering, Trends, Researches and Technologies*, Anthony N. Laskovski, pp. 203-224. InTech, ISBN 978-953-7619, Rijeka, Croatia

Zhang, F.; Adam, M.; Otterstein, E.; Burkel E. (2011). Pulsed electric field induced diamond synthesis from carbon nanotubes with solvent catalysts. *Diamond and related Materials*. 20: 853–858

Zhang, F.; Mihoc, C.; Burke E. (2010). Spark plasma sintering assisted carbon conversion from various modifications to diamond. *Conference Proceedings of Materials Science and Technology (MS&T) 10,* pp. 2312-2317, ISBN 978-0-87339-756-8, Houston, TX, USA, October 17-21, 2010

Zhang, F.; Mihoc, C.; Ahmed, F.; Latte, C.; Burkel, E. (2011). Thermal stability of carbon nanotubes, fullerene and graphite under spark plasma sintering. *Chemical Physics Letters*. 510:109-114

Zhang, F.; Ahmed, F.; Holzhüter, G.; Burkel, E. (2011). Growth of diamond from fullerene C60 by spark plasma sintering. *Journal of Crystal Growth*. doi:10.1016/j.jcrysgro.2011.11.01494

Zhang, F.; Burkel, E.; Rott, G. (2011). Verfahren zur synthese von diamanten. *Deutsches Patent*. P162-11

Zheng, Z.; Liao, L.; Yan, B.; Zhang, J. X.; Gong, H.; Shen, Z. X.; Yu, T. (2009). Enhanced field emission from argon plasma-treated ultra-sharp *a*-Fe_2O_3 nanoflakes. *Nanoscale Res Lett*. 4:1115–1119